Glass Buttes Exploration and Drilling Project

MERGING HIGH RESOLUTION GEOPHYSICAL AND GEOCHEMICAL SURVEYS TO REDUCE EXPLORATION RISK AT GLASS BUTTES, OREGON

Final Report

DE-EE0002836

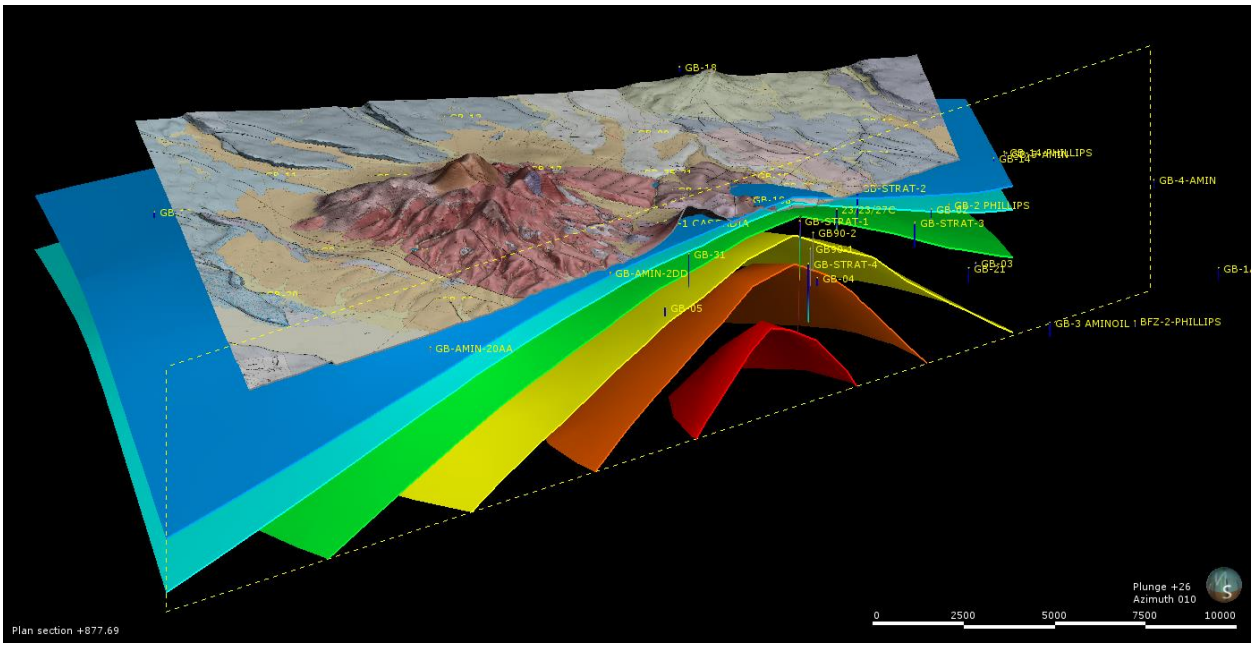

United States Department of Energy – Geothermal Technologies Program
Ormat Nevada, Inc.

Patrick Walsh, Steven Fercho, Doug Perkin, Ormat Nevada, Inc.
Brigette Martini, Corescan Inc.
Darrick Boshmann, Oregon State University

Table of Contents

Table of Figures

1.0 Executive Summary

The engineering and studies phase of the Glass Buttes project was aimed at reducing risk during the early stages of geothermal project development. The project's inclusion of high resolution geophysical and geochemical surveys allowed Ormat to evaluate the value of these surveys both independently and in combination to quantify the most valuable course of action for exploration in an area where structure, permeability, and temperature are the most pressing questions. The sizes of the thermal anomalies at Glass Buttes are unusually large. Over the course of Phase I Ormat acquired high resolution LIDAR data to accurately map fault manifestations at the surface and collected detailed gravity and aeromagnetic surveys to map subsurface structural features. In addition, Ormat collected airborne hyperspectral data to assist with mapping the rock petrology and mineral alteration assemblages along Glass Buttes faults and magnetotelluric (MT) survey to try to better constrain the structures at depth. Direct and indirect identification of alteration assemblages reveal not only the geochemical character and temperature of the causative hydrothermal fluids but can also constrain areas of upflow along specific fault segments. All five datasets were merged along with subsurface lithologies and temperatures to predict the most likely locations for high permeability and hot fluids.

The Glass Buttes temperature anomalies include 2 areas, totaling 60 km^2 (23 mi^2) of measured temperature gradients over 165° C/km (10° F/100ft). The Midnight Point temperature anomaly includes the Strat-1 well with 90°C (194 °F) at 603 m (1981 ft) with a 164 °C/km (10°F/100ft) temperature gradient at bottom hole and the GB-18 well with 71°C (160 °F) at 396 m (1300 ft) with a 182°C/km (11°F/100ft) gradient. The primary area of alteration and elevated temperature occurs near major fault intersections associated with Brothers Fault Zone and Basin and Range systems. Evidence for faulting is observed in each data set as follows. Field observations include fault plane orientations, complicated fault intersections, and hydrothermal alteration apparently pre-dating basalt flows. Geophysical anomalies include large, linear gradients in gravity and aeromagnetic data with magnetic lows possibly associated with alteration. Resistivity low anomalies also appear to have offsets associated with faulting. Hyperspectral and XRF identified alteration and individual volcanic flow units, respectively. When incorporated into a 3D geologic model, the fault intersections near the highest proven temperature and geophysical anomalies provide the first priority targets at Midnight Point.

Ormat geologists selected the Midnight Point 52-33 drilling target based on a combination of pre-existing drilling data, geologic field work, geophysical interpretation, and geochemical analysis. Deep temperatures of well 52-33 was lower than anticipated. Temperature gradients in the well mirrored those found in historical drilling, but they decreased below 1500 ft and were isothermal below 2000 ft.

2.0 Introduction

In December 2008, Ormat acquired BLM leases at the Glass Buttes Prospect, Lake County, Oregon. Following preliminary investigations including geologic field work and literature review, Ormat applied for Department of Energy Innovative Exploration Technologies Program. Ormat chose to propose this prospect because it provides a field laboratory with a unique geothermal environment, as described in the following sections. An innovative suite of high resolution geophysical and geochemical techniques will reduce exploration drilling risk by characterizing fault geometries and relationships. From a resource perspective, temperature and permeability are the greatest risk factors in geothermal development. This report is intended to describe how Ormat used the exploration surveys to finalize the first drilling locations, which are intended to minimize these risks.

We have acquired high resolution LIDAR data to accurately map fault manifestations and lithologic relationships at the surface and collected detailed gravity and aeromagnetic surveys to map subsurface manifestations. We also collected airborne hyperspectral data to map rock petrology and mineral alteration assemblages along these faults. Alteration assemblages reveal not only the geochemical character and temperature of the causative hydrothermal fluids but also may constrain areas of upflow along specific fault segments. Initial interpretations of these data sets were extremely valuable, but they also showed ambiguous and sometimes conflicting structures. Following completion of the planned surveys, Ormat added a magnetotelluric (MT) survey to try to better constrain the structures at depth. All five datasets have been interpreted and merged along with subsurface lithologies and temperatures from previous wells to predict the most likely locations for high permeability and hot fluids. We have used the identified locations to site two slim holes to test the resource model. The slim holes will be drilled with a core rig to 3000 to 4000 feet deep. If either well is encouraging, we plan to drill a production size well to prove the resource.

2.1 Glass Buttes geologic background

The Glass Buttes project area is characterized by a complex of silicic volcanism approximately 5-6.5 million years old that interfingers with and is overlain by basalt flows and alluvium. Field observations show that young faults associated with WNW-trending Brothers Fault Zone (BFZ) and NNE-trending Basin and Range deformation deform all of these rock units. The BFZ is an extensive WNW trending fault system at the northern terminus of the basin and range. Normal to right-lateral oblique faults deform young volcanics and sediments from Alvord Desert to Newberry Crater with increasing younger silicic volcanism toward the northwest.

The silicic volcanism at Glass Buttes is most likely too old to be associated with the observed geothermal anomaly, but previously native deposition of mercury and advanced argillic alteration assemblages observed at the surface and described in drilling reports indicate that high temperature fluids have migrated through the system more recently (e.g., (Berri, 1982) (Johnson M. J., 1984). Alteration age is unknown but appears to occur along young faults. More recent field mapping by Boschmann (2012) identified stratigraphic constraints that may indicate near-surface hydrothermal alteration associated with mercury ores ceased before 4.70±0.27 Ma, and is likely associated with the 6.49±0.03 Ma rhyolite eruptions in the eastern part of Glass Buttes. Spectral-based alteration mapping shows pervasive regional weathering assemblages punctuated by distinct linear trends of hydrothermal assemblages coincident with these faults. Temperature measurements indicate that the area maintains a thermal anomaly with >10°F/100ft gradients observed at bottom hole in both shallow- (<500ft) and intermediate-depth (<2000 ft) wells (e.g., (Benoit, 1981); (Johnson & Ciancanelli, 1989); Figures 1 and 2).

Ormat's geologic model includes fluids circulating along deep portions of the younger faults and possibly lithologic boundaries with upflow along fault intersections in the Midnight Point area. Our exploration program includes geologic and geophysical work and structural modeling prior to drilling that will test several geologic models for permeability and fluid migration. These models require the Glass Buttes project to be divided into 2 areas. In the Midnight Point area, we will test faults and fault intersections internal to the silicic volcanism. These faults include WNW-ESE BFZ faults, N-S faults that may be associated with Basin and Range extension, and the intersection of these systems. The drilling in the late 1970s (Phillips, Francana, and Aminoil) showed that both Midnight Point and the Mahogany areas have anomalous heat flow and thermal gradients. Midnight Point is considered lower risk and higher priority due to having more

drilling data, a more complicated fault system, better fault orientation constraints, extensive volcanic vents associated with faulting, and surface alteration.

2.2 **Prospect History**

Phillips Petroleum discovered this potential resource in the late 1970s using widely spaced gradient holes and a few intermediate-depth (<2000 ft) wells in one area. This type of large-scale exploratory drilling is no longer possible due to budget and permitting constraints. Phillips temperature gradients indicate economic temperatures shallower than 4000 ft (Figures 1 and 2). Phillips did not find flowing water, largely due to the lack of structural model and absence of a deeper drilling program. However their shallow and intermediate depth drilling highlighted two large areas that deserve renewed exploration. The combined areas are ~60 km^2 (~23 mi^2) with over 164 °C/km (10°F/100ft).

Ormat acquired BLM and OR State leases in 2008 and 2009. The collaborative technical effort between Ormat geologists and Oregon State professors and students has been ongoing since 2009. Permitting of potential drill sites has been delayed by biological and cultural concerns.

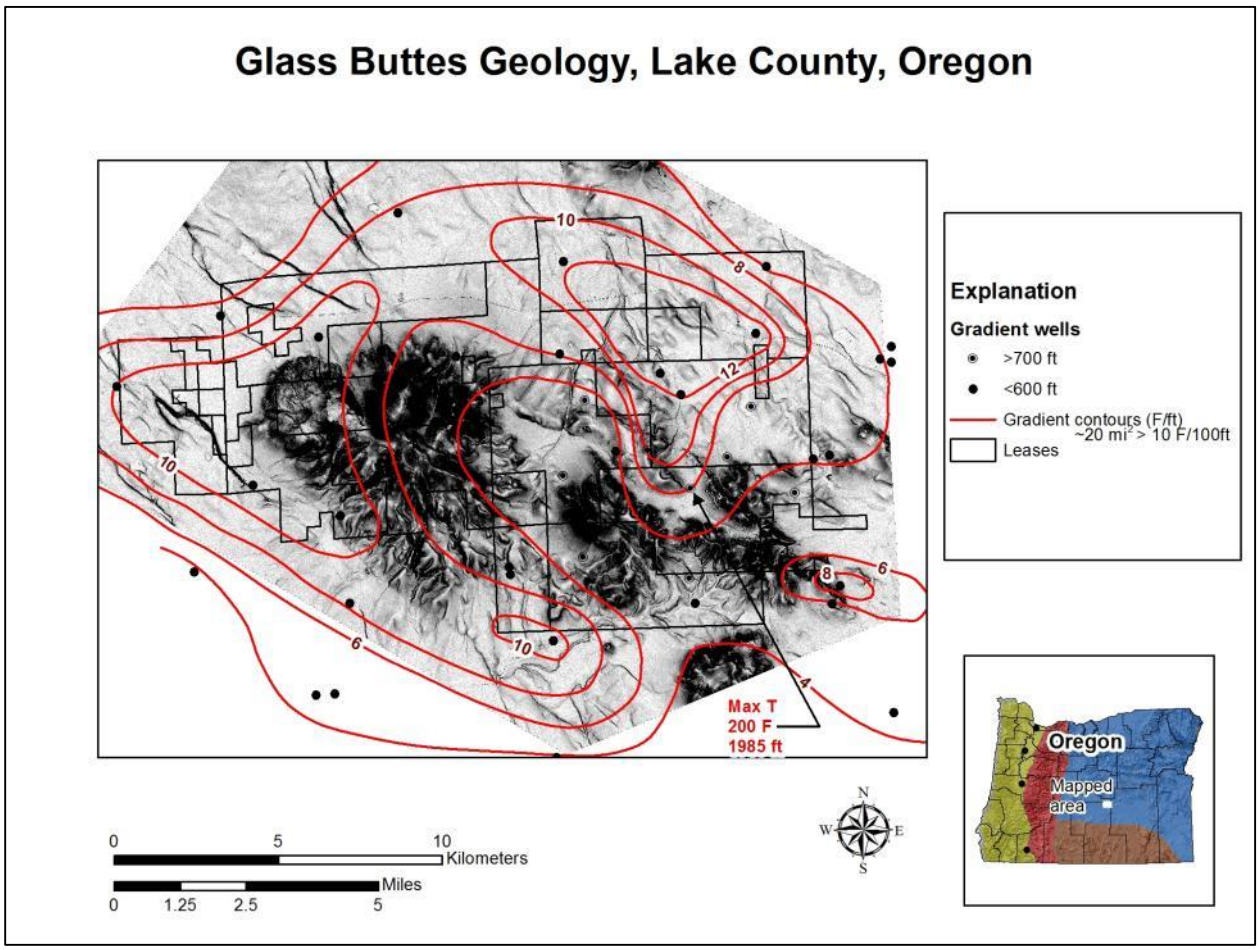

Figure 1. Glass Buttes, Oregon map with LiDAR slope shade background and temperature gradient contours.

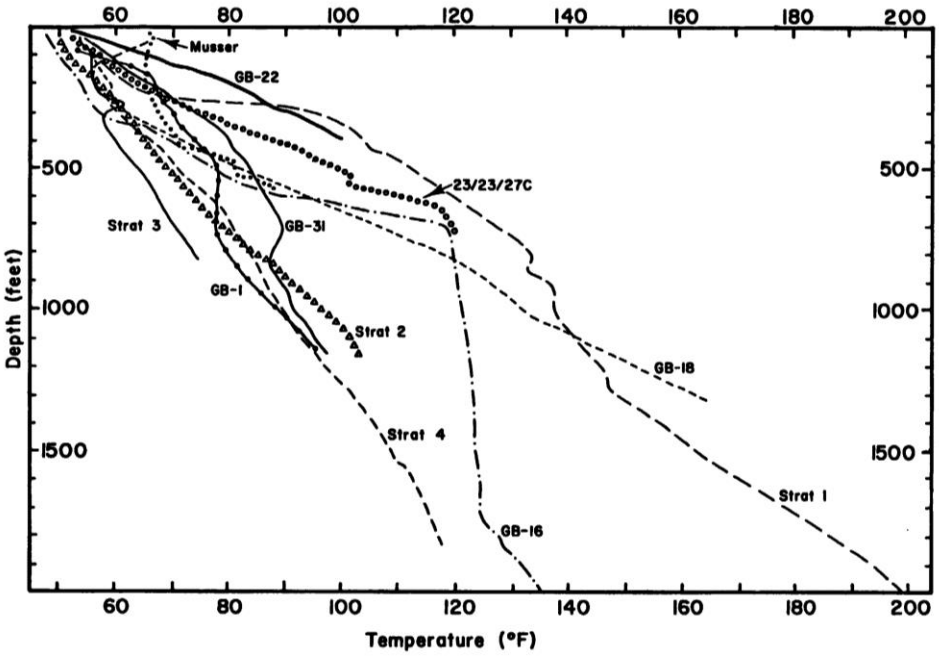

Figure 2. Temperature logs from intermediate-depth drilling (Johnson & Ciancanelli, 1989).

3.0 Results of exploration surveys

3.1 Field Mapping

Darrick Boschmann conducted two years of field mapping and analysis (Boschman, 2012). Initial mapping efforts focused on the Parmele Ridge relay structure (Potato Lake Quad: 43.5540N, 120.1455W) West of Glass Butte and the Midnight Point prospect (Burns Quad: 43.5482N 119.9761W) to the East. Previous field mapping at Glass Buttes (e.g. (Roche, 1987), (Johnson M. J., 1984), (Berri, 1982)) described a series of late Miocene to Pliocene silicic domes and vents intercalated with minor basaltic lavas and unconformably overlain by a series of Plio-Pleistocene age basaltic lavas sourced from around and within the Glass Buttes complex. Silicic facies include rhyolite, rhyodacite and obsidian flows, pumice, breccia, pyroclastic rocks and volcaniclastic sediments. Radiometric age dates of 6.49 ±0.03Ma (Ar/Ar), 5.79 ±0.02Ma (Ar/Ar), and 5.04 ±0.75Ma (K/Ar) place the eruption of silicic units in the late Miocene ((McKee & Walker, 1976), (Jordan, Grunder, Duncan, & Deino, 2004), (Ford)). Basaltic vents and flows are found around and within the silicic complex and also comprise the surrounding plateau. Age dating and crosscutting relationships from this study indicate that basaltic eruptions from numerous small

mafic vents continued from >6.49±0.03 Ma to 1.39±0.18 Ma.(Jordan, Grunder, Duncan, & Deino, 2004).

Exposed fault surfaces are rare, but where found yield dip measurements of 66-71° with slickenlines pitching 65-90° indicating primarily normal to slightly oblique slip along these faults. Crosscutting and stratigraphic relationships allow us to begin unraveling the relative tectonic and volcanic development of the Glass Buttes area. Lidar facilitated improved accuracy in field mapping, (Figure 3) and (Figure 9) illustrate a few examples. The oldest rocks (Tr) are a series of rhyolite flows and domes with facies varying from dense aphyric stony interiors to rhyolite and obsidian flows to pumiceous and pyroclastic aprons with local obsidian blocks. These are interpreted as distinct facies of single eruptive centers. As these units weathered, fluvial processes transported material down slope, depositing alluvium consisting of subangular-subrounded clasts of obsidian, pumice and rhyolite along the flanks of the dome (Qoa: older alluvium). A series of basalt flows (Tb1) erupted onto this sedimentary surface before a set of NW striking normal faults developed with fault planes dipping to the NE. This set of faults was in turn cut by a set of NE striking faults dipping to the NW resulting in an apparent dextral separation of the NW striking scarps. These NE striking faults are not observed to offset NW striking faults to the south, suggesting a second period of NW striking faulting or concurrent motion on both sets. Continued erosion and deposition of Qoa concealed geomorphic evidence of faulting in much of the area. At least two basalt flows (Tb2, Tb3) erupted to the west and north of the mapping area, burying parts of both some NW and NE trending faults.

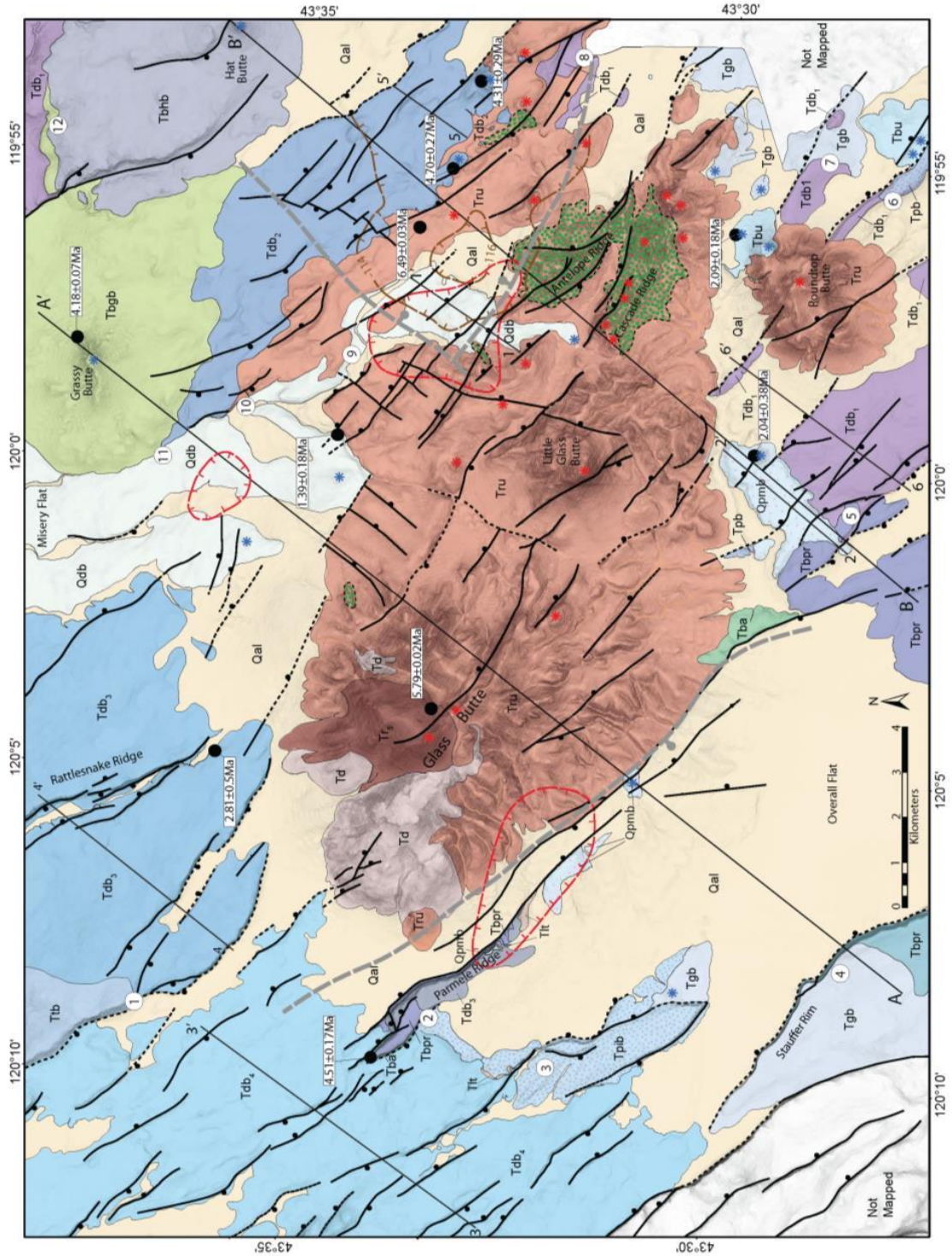

Figure 3. Simplified geologic map. Red hatched lines indicate 165° C/km (10° F/100ft) temperature gradient anomalies in the eastern (Midnight Point) and western (Mahogany) areas (Boschman, 2012).

3.2 Remote Sensing

3.2.1 LiDAR

Ormat contracted Watershed Sciences, Inc. to collect approximately 84,849 acres of Light Detection and Ranging data (LiDAR) (Figure 4). The products of this survey are 1-meter resolution elevation models that are processed for first return and bare ground. The first return model includes vegetation while the bare ground has had vegetation removed. The LiDAR survey also provides a 0.5-meter resolution intensity image, which is basically a high resolution air photo that can be draped over the elevation models or used as a map background. These models and images can be combined for vegetation studies but are not used for that purpose in this project. Future studies may include attempting to correlate the LiDAR intensity image with the Hyperspectral data to determine if the LiDAR may provide an additional avenue of research for these data sets.

The high-resolution elevation data are being used to increase the accuracy of geologic mapping and to site drill locations. The geologic mapping is improved because features such as minor breaks in slope can be used to better define a lithologic contact or subtle fault that would not be clearly identified using traditional methods. The LiDAR data have also been very valuable in defining cross-cutting relationships and therefore relative ages of geologic features. These geologic interpretations are explained further in section3.1, Field Mapping. The LiDAR data are also being used to site well surface locations in 2 ways. The first is a basic slope map where we can choose well pads based on low slope values to minimize required disturbance. The second is by creating viewshed maps to avoid drilling where Sage Grouse could see the operations (Figure 5)

Preliminary structural analysis of the Glass Buttes area was conducted beginning in July and August 2010 using the 1-meter resolution Light Detection and Ranging (LiDAR) data acquired in June, 2010 and processed to produce a bare earth model. LiDAR based fault mapping is an effective method for identifying subtle surface expressions of fault zones (e.g. Haugerud et al. (2003)). Faults, fractures, and volcanic vents were digitally mapped using ArcGIS software. Fault and volcanic vent identification was facilitated by variable illumination hillshading, elevation contouring and slope analysis tools including slope mapping and slope-shade visualizations. Vents were identified by the presence of local topographical highs or distinguishable fissures in association with lava flow textures. Faults were identified by steep topographic scarps, laterally continuous steep slopes, linear breaks in slope, alignments or offsets in topographic features or

the presence of regular and continuous morphological breaks. Fault traces were digitized as line shape files and attributed with length, azimuth, downthrown direction and midpoint location.

The results of the preliminary structural LiDAR analysis (Figure 6) are in general agreement with the previously described structural fabric of the Brothers Fault Zone (Lawrence, 1976). The area is dominated by low to moderate displacement (<60 m throw), NW striking, often en echelon faults with apparent normal separation. Volcanic vents tend to align along these NW striking faults. A smaller population of NE striking faults locally cross cuts the NW striking set, resulting in an apparent dextral separation of NW striking scarps (Figure 7) (Figure 9). Well-developed relay ramps occur at several locations where sub-parallel fault segments overlap in map view (Figure 8). Relay structures transfer displacement between overstepping fault segments and can be breached producing a continuous fault with an along-strike bend (Peacock & Sanderson, 1994). Comparison of fault traces and volcanic vents identified here using LiDAR imagery to those previously identified at Glass Buttes illustrates that many additional faults and vents can be identified using high resolution LiDAR.

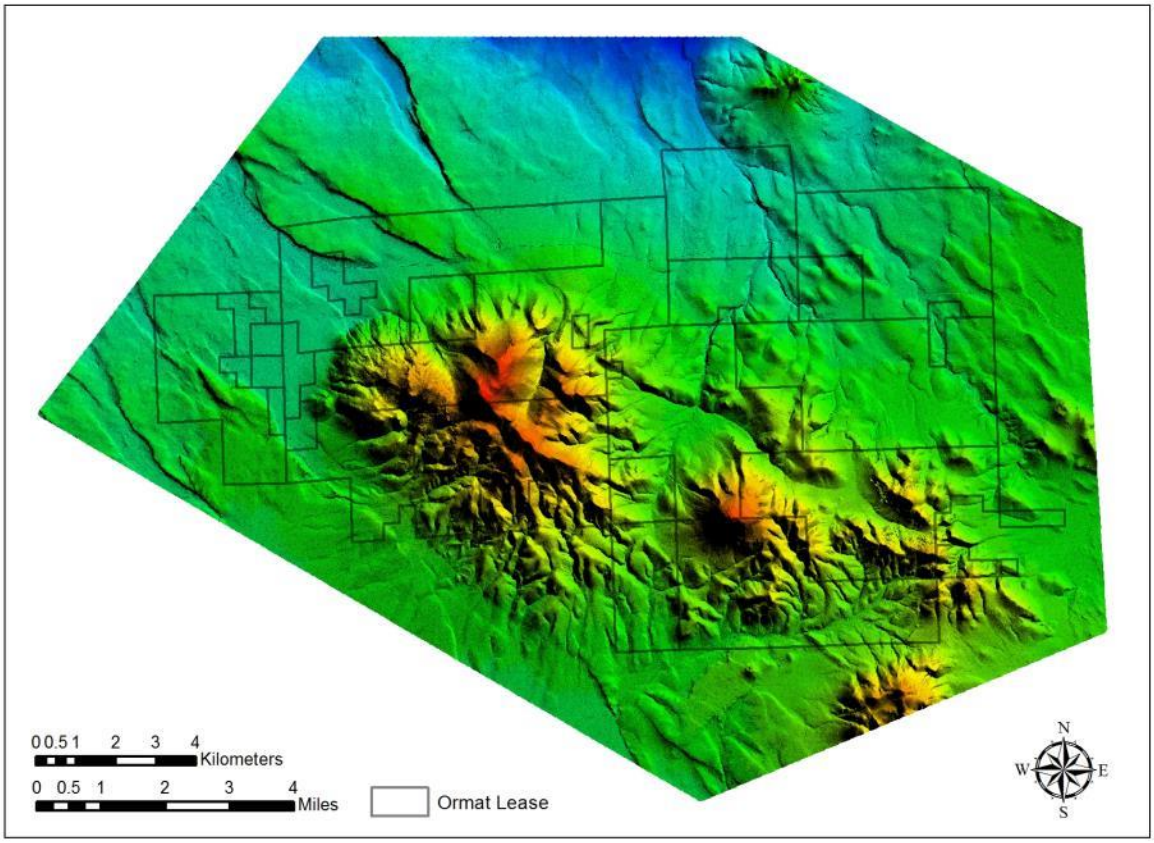

Figure 4. Shaded relief map with colored elevation, both based on Lidar data, and lease outlines.

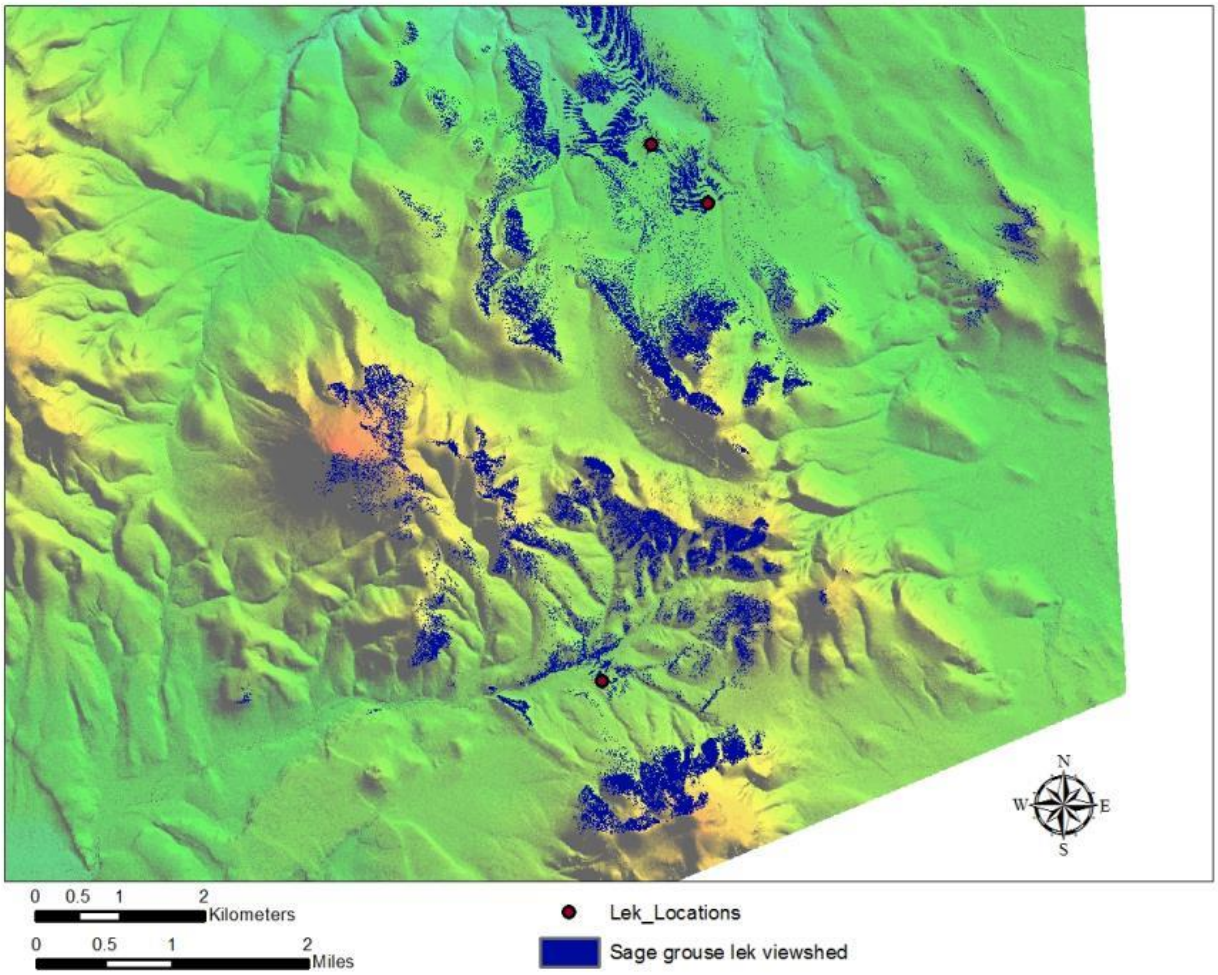

Figure 5. Lidar Elevation map with processed sage grouse viewshed at Midnight Point.

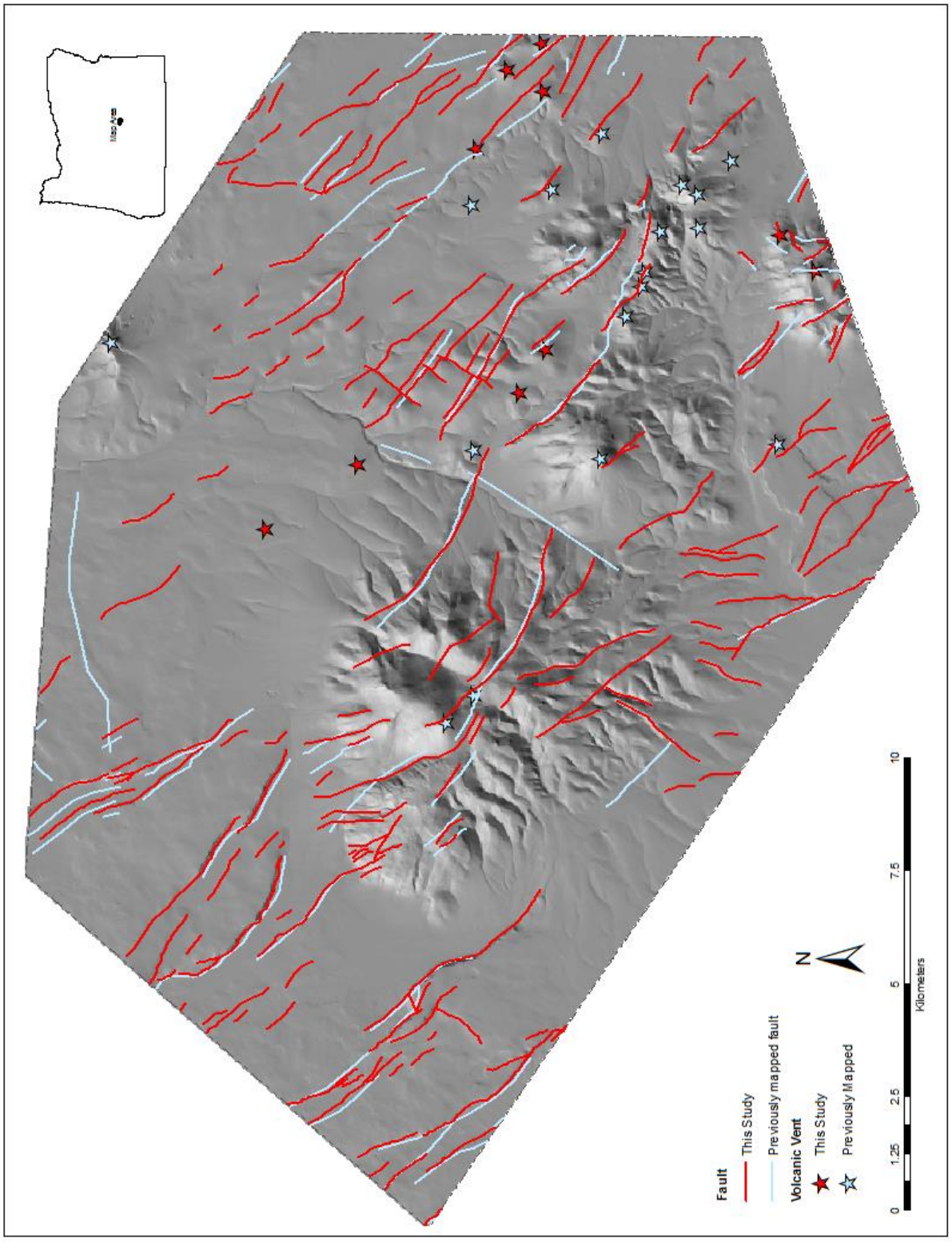

Figure 6. Structural map of the Glass Buttes volcanic complex and LiDAR based hillshade.

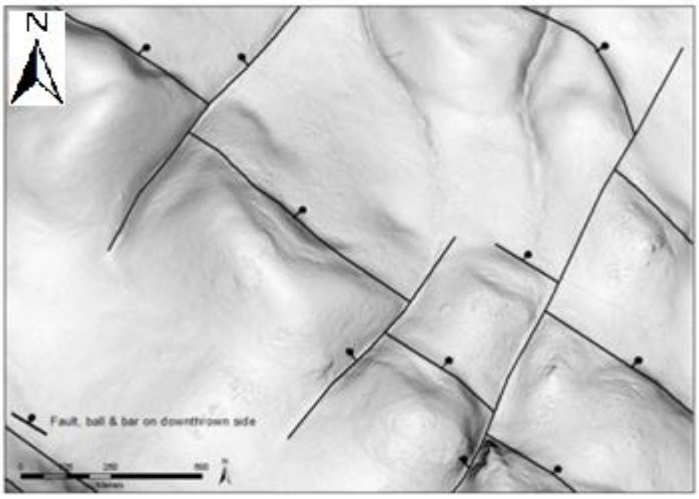

Figure 7. LiDAR slope-shade map illustrating cross cutting relations between NE and NW striking faults. NE striking faults cut individual NW striking faults resulting in an apparent dextral separation. Subsequent NW striking faults are not observed to be cut by these NE striking faults. This type of relationship suggests some degree of cogeneity of the two fault populations.

Figure 8. LiDAR slope-shade map of a well-developed relay ramp between two en echelon (overlapping) fault segments. Vertical separation on both segments is <40m decreasing to zero as they enter the overlap zone. The two faults here are soft linked; i.e. they are not connected across the ramp by a continuous fault, leaving an active ramp (Crider & Pollard, 1998). Displacement increase along the two segments will produce strain in the ramp resulting in fracturing and eventually formation of a ramp breach fault connecting the two segments (Peacock & Sanderson, 1994).

Figure 9. Example of results of new geologic mapping illustrating local structural and volcanic development. Tb3, a single basalt flow sourced just west of the map area buries and post-dates the NW striking fault at point A. Tb2, a series of at least 3 individual basalt flows sourced to the east of the map area overlies the NE striking fault at point B. A third series of basalt flows, Tb1 is cut by the NW striking fault at point C. Tr = rhyolite & obsidian flows, Qoa = older alluvium, Qal = Quaternary alluvium. Black lines = faults with ball on downthrown side.

3.2.2 Hyperspectral data

Hyperspectral data (HyMap, Integrated Spectronics Pty., Sydney, Australia) was flown over the Glass Buttes leases on 19 August 2009; a total of 14 lines of data were acquired covering an area just under 300 mi^2 (Figure 10). The HyMap is an airborne hyperspectral scanner delivering 126 bands (approx. 18 nm width per band) of imagery over the 450 nm to 2500 nm spectral interval. Spatial resolution is nominally 3 m, though resolution changes slightly with topography. Data

were delivered as radiance and apparent reflectance and were cross track and level corrected, i.e. solar illumination corrected to account for systematic opposing flight directions. A Geographic Lookup Table (GLT) file was also delivered for aid in subsequent geometric rectification / mosaicing. Each reflectance image was geo-corrected to position each individual pixel in its accurate geo-location in the UTM/WGS 84 map projection. The corrected image strips were then mosaiced to produce seamless, homogeneous data for the whole survey area.
This data-cube was then processed to produce a series of spectral-based maps showing contiguous surface material distribution of minerals and vegetation. Processing schemes aimed at highlighting mineralogical and geological/chemical variations included band color composites, minimum noise fraction (MNF), band ratio index images, and spectral un-mixing images.

A total of 11 spatially coherent mineral species were identified over the lease area that distinctly map 7 unique minerals, i.e. there are multiple end members of some minerals. Identified minerals include Dickite (a high temperature form of kaolinite), Alunite (a high temperature aluminum-rich sulfate), Kaolinite, Sericite, Opal (likely representative of the ubiquitous obsidian flows), Goethite (a water-rich iron-oxide) and Tourmaline (a hydrothermal silicate). Two 'types' or end members of Dickite were identified; differences may be due to temperature of formation and/or mixing with kaolinite. Four end members of Opal were identified; it is likely this has to do with innate differences with the obsidian flows themselves and is not related to secondary hydrothermal deposition. Extensive field work and lab spectroscopy outside the scope of this project would be required in order to confirm or exclude this theory.

The distribution of mineral assemblages is markedly different from west (Mahogany) to east (Midnight Point). Some of the differences in distribution are clearly due to advanced levels of disturbance (mainly mining activities) seen in the eastern portion of the leases. However some of the differences are undoubtedly inherent to the parent hydrothermal system. The dominant assemblages in the east are characteristic of advanced argillic phase alteration from secondary hydrothermal alteration (Figure 11). While the presence of dickite alone is not proof of a hydrothermal genesis, its co-occurrence with alunite (and to an extent, tourmaline) indicates hydrothermal deposition. We also see the typical 'bullseye' zonation patterns inherent to hydrothermal alteration (similar to those assemblages and patterns seen in epithermal mineral deposits); higher temperature alunite surrounded by lower temperature dickite and kaolinite. These assemblages are more obvious in the areas that have been actively 'scraped' and mined, but the dickite/alunite assemblage is found extensively over much of the eastern lease in areas

that have received no human disturbance. Furthermore, the distribution of these assemblages are clearly aligned and/or concentrated along both known and recently mapped structural features. The character of the alteration and it's co-location with structural weaknesses (faults and fractures) is concrete proof that a hydrothermal system operated within the Glass Buttes geologic province at one time. Unfortunately, this data cannot reveal age of alteration formation, only its absolute identity and distribution.

In contrast to Midnight Point, alteration distribution at Mahogany is quite different and nowhere near as prolific. In fact the dominant minerals mapped in the west are the various opal end members (Figure 12). Of course it is likely that these opal minerals are in fact mapping obsidian outcrops rather than secondary opaline deposition; spectrally discriminating opal from obsidian would be very difficult to impossible. In addition to opaline end members, there are limited distributions of kaolinite/dickite/alunite at Mahogany. These small patches of advanced argillic alteration do not appear to be associated with human disturbance and in at least one case, co-occur with a mapped fault. In general, there is a sparse 'salt and pepper' distribution of dickite throughout the western area – however most is not present in any density like that seen on the east side. Several possibilities exist: 1) A hydrothermal system has never Mahogany, 2) A western hydrothermal system has existed or does exist at depth and thus shows no surface expression and 3) All evidence of hydrothermal alteration has been removed or weathered away. The fact that limited patches of alteration are seen at Mahogany seems to indicate that possibility one (1) is false. It is more likely that a combination of possibilities two and three (2 & 3) are true, and either way, indicates that accessing a potential reservoir at Mahogany may require deeper drilling. Field mapping supported by this airborne hyperspectral mineral mapping found that unaltered unit Tdb2 overlies hydrothermally altered silicic rocks ~3 kilometers northeast of Antelope Ridge. Accordingly, one hypothesis is that hydrothermal alteration is likely related to the emplacement and eruption of the silicic volcanic centers at the eastern end of the complex, dated at 6.49±0.03Ma (Boschmann, 2012).

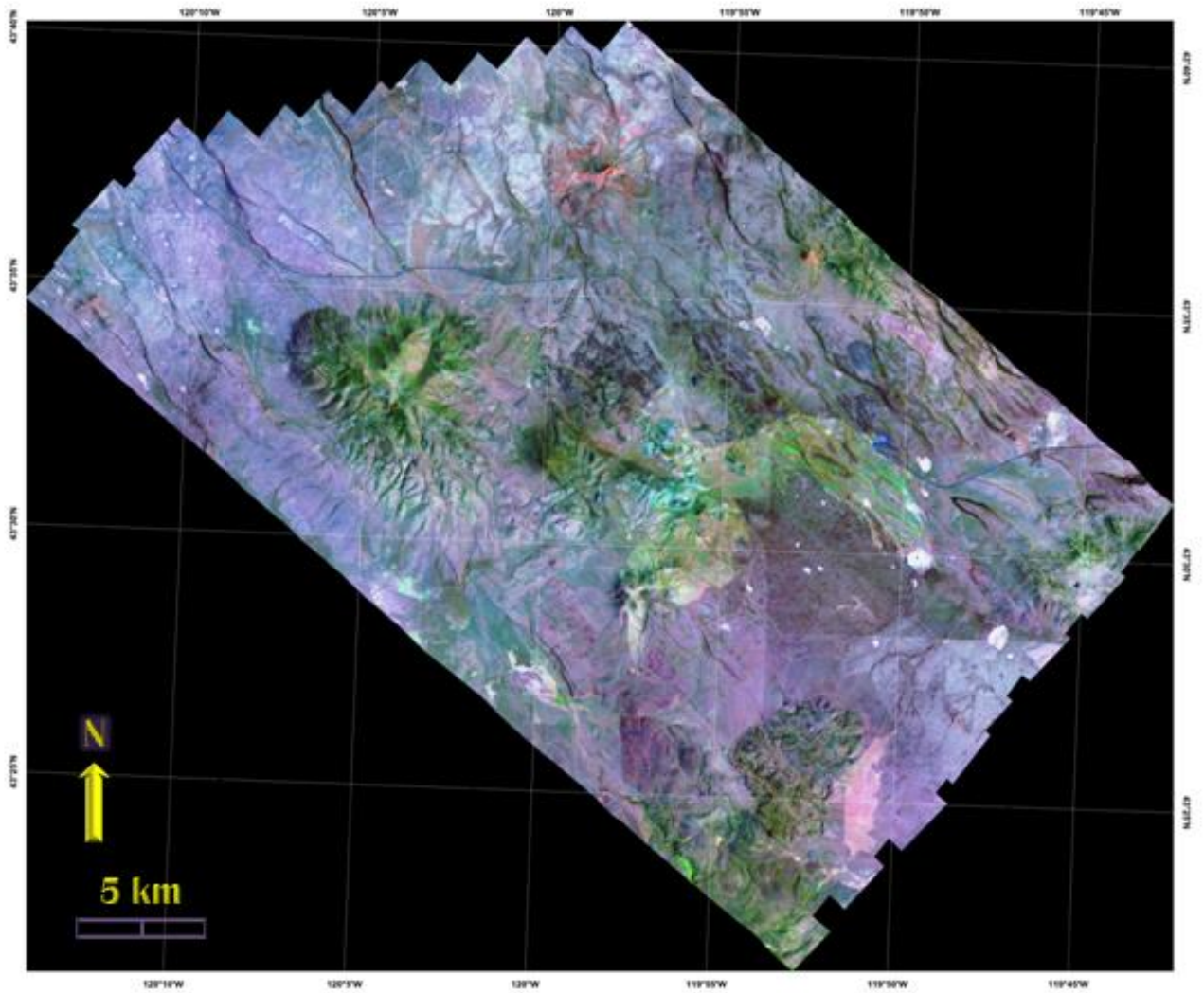

Figure 10. HyMap Hyperspectral data over the Glass Buttes leases displayed as a false color image. Pixels dominated by vegetation appear green, soil/rock appears reddish/brown and water appears blue. Extremely bright, disturbed areas will appear white to light blue/cyan.

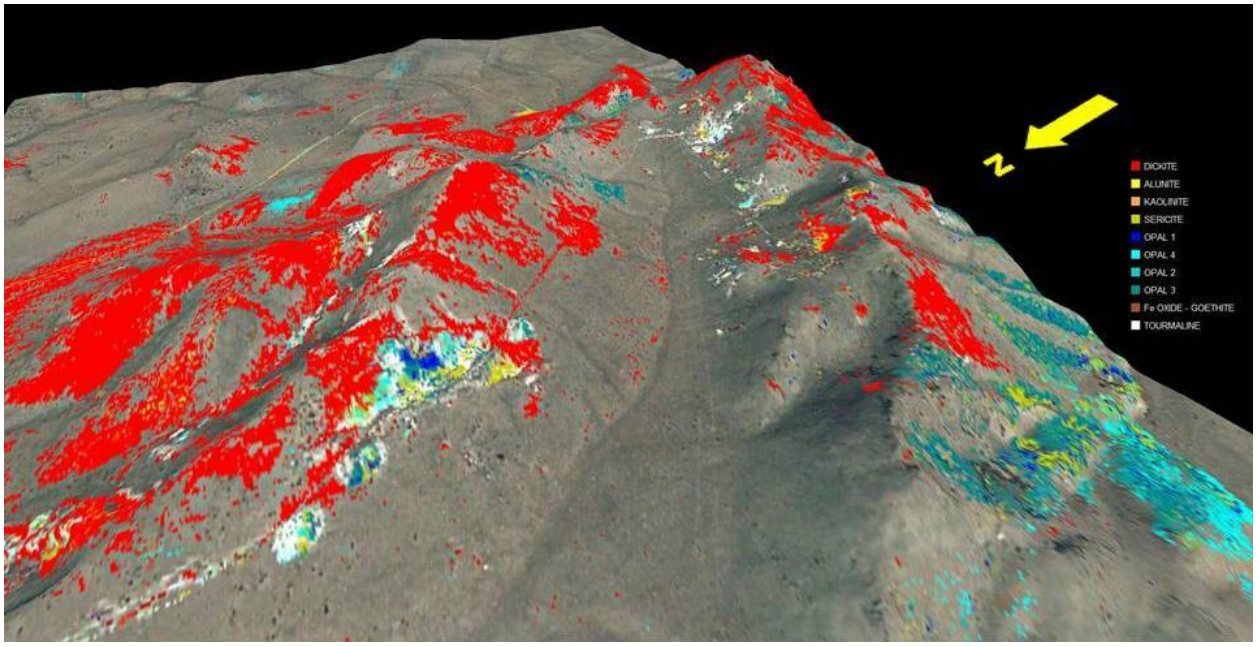

Figure 11. Mineral alteration distribution on the eastern leases (Midnight Point). Alteration measured from airborne hyperspectral data is mapped on 1 m color imagery which is in turn draped on 1m LiDAR imagery for elevation.

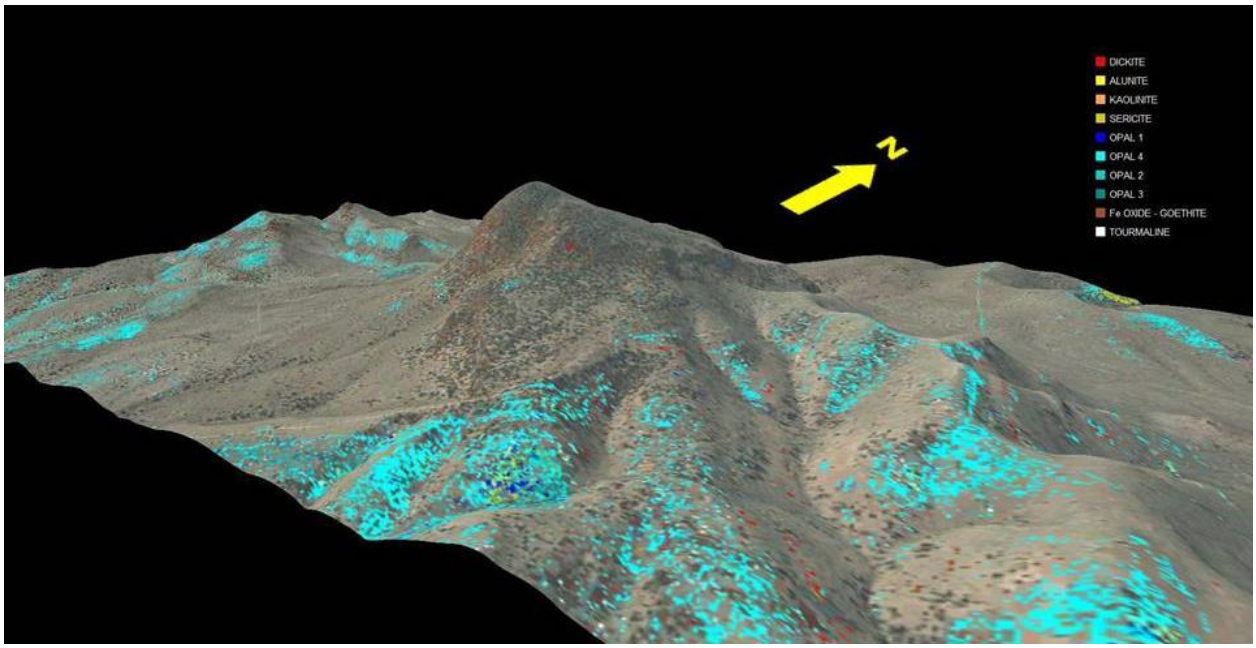

Figure 12. Mineral alteration distribution on the western leases (Mahogany). Alteration measured from airborne hyperspectral data is mapped on 1 m color imagery which is in turn draped on 1m LiDAR imagery for elevation.

3.3 Geophysical Surveys

3.3.1 Gravity

3.3.1.1 Gravity data collection and processing

Ormat contracted Zonge Geosciences to collect 355 gravity stations in 2009 along existing roads, followed by an additional 182 stations for more detailed work in 2010, for a total of 537 gravity stations (

Figure 13). The added stations made 5 transects across broad gradients to see if they could be better resolved. Zonge processed these data to remove effects from instrumentation (e.g. drift), position (latitude and surface elevation), earth curvature, and earth tides to reduce the data to effects only associated with subsurface density variation. The results following the additional stations were similar to the original process data and only the final data are presented here.

Figure 13 illustrates the Complete Bouguer Anomaly, representing only the effects of subsurface density contrasts. Figure **14** illustrates the Horizontal Gradient Magnitude of the Complete Bouguer Anomaly. The horizontal gradient is used to identify linear features that can be interpreted as subsurface faults.

3.3.1.2 Gravity data interpretation

On the western side of Glass Buttes, a northwest striking gravity gradient has a fairly steep, 5 km-wide decrease from -105 to -120 mgals. Similarly, on the eastern side, a northeast striking gravity gradient has a 4 km-wide decrease from -107 to -116 mgals (**Figure 14**). Both of these trends have horizontal gradient anomalies of similar widths. The initial interpretation was that these trends indicate deep-seated faults that dip away from the Glass Buttes complex. Modeling was challenging because of the non-unique nature of the apparent faults. Almost any combination of number of faults, dip, and location could recreate a similar pattern (e.g. Figure 15), and this problem was more difficult on the west side than on the east side. However other geophysical methods and field mapping are more consistent with the second complicated graben model shown in figure 15. On the east side the anomalous gradient was found to represent three separate structures dipping away from the Glass Buttes complex, which will be discussed in the Integrated analysis of results section.

On the western side the primary northwest trending structure has an abrupt left, possibly dextral, step at arrow shown in

Figure 13. The arrow marks a fault intersection that corresponds with the central portion of the main Glass Buttes rhyolitic dome, and may have been the control on that domes emplacement. This hypothesis is explored further in the sections on Aeromagnetic survey interpretation and Integrated analysis of results.

On the eastern side the primary northeast trending structure intersects a WNW trending structure near the star shown in

Figure **13**. This intersection is immediately west of the mapped hydrothermal alteration as seen in the hyperspectral data and described by (Johnson & Ciancanelli, 1989) (Johnson M. J., 1984) (Berri, 1982). This intersection, its proximity to surficial alteration and known temperature anomalies make it one of the primary targets for Phase II drilling.

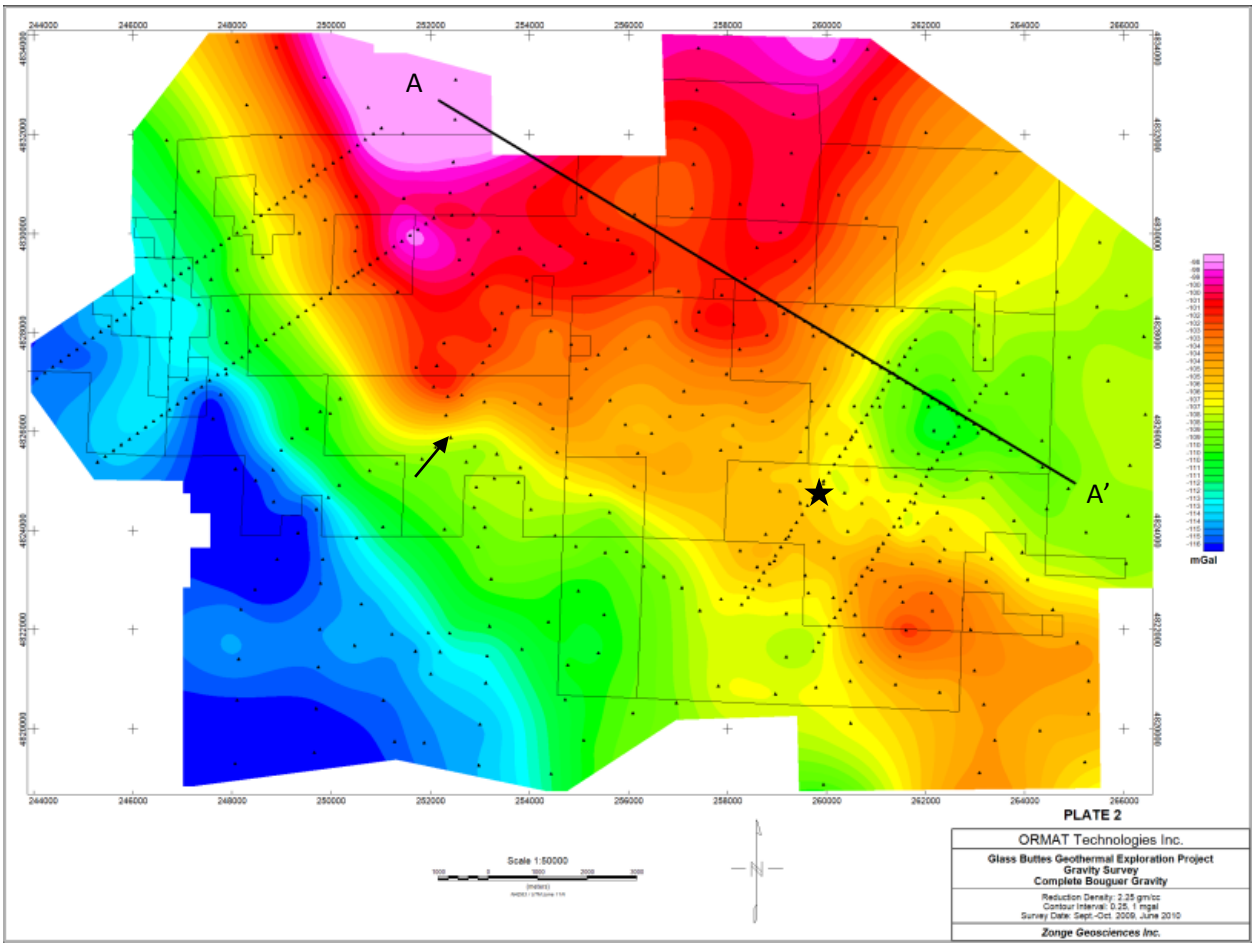

Figure 13. Complete Bouguer gravity calculated with a reduction density of 2.25 gm/cc. Individual stations are marked.

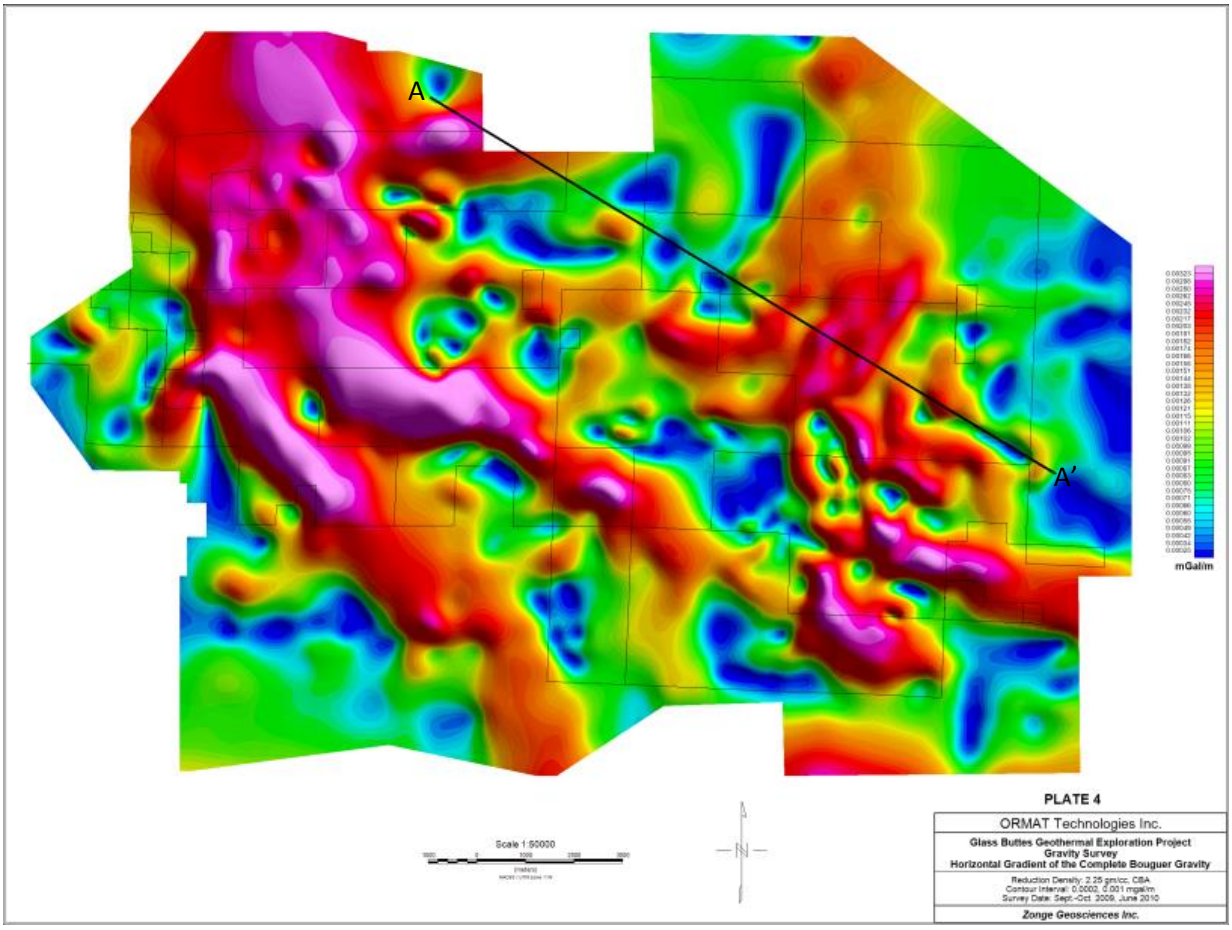

Figure 14. Horizontal gradient magnitude of the Complete Bouguer gravity calculated from data shown in Figure 15.

a) **Glass Buttes Profile 4. V1**

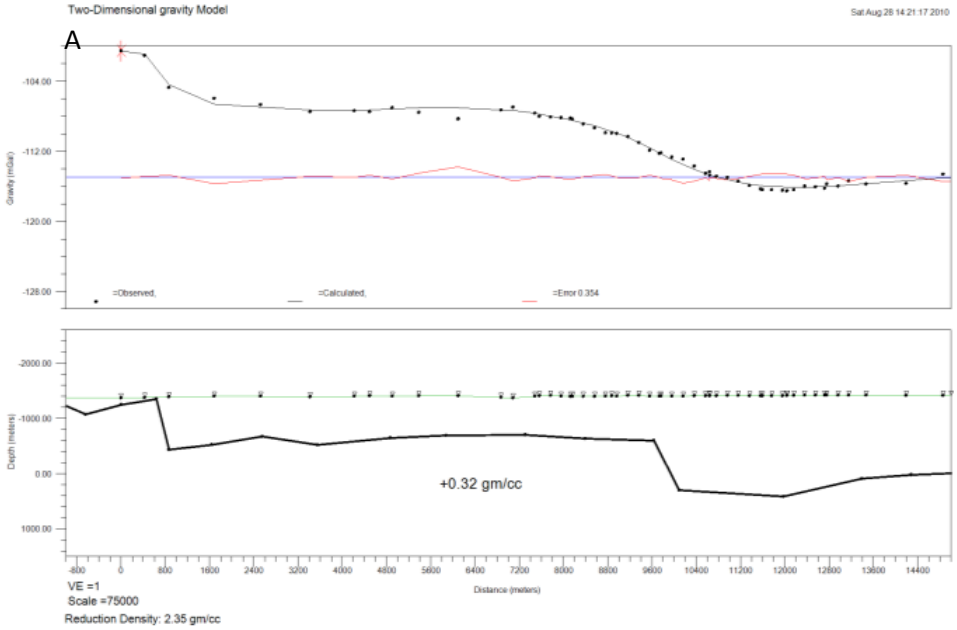

b) **Glass Buttes Profile 4, V2**

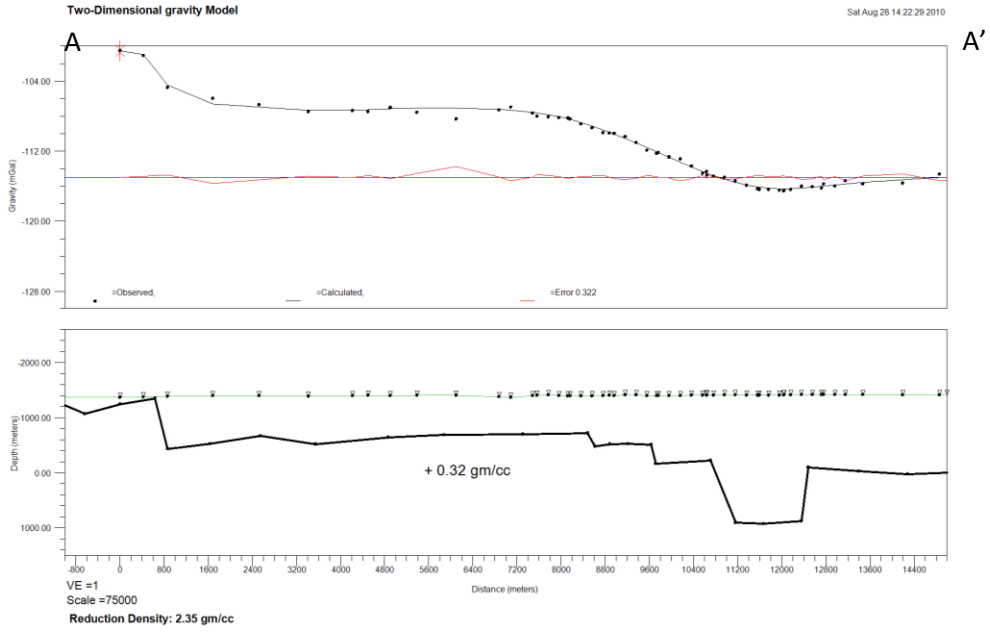

Figure 15. Sample model cross sections A-A'. Location shown on

Figure 13**. A) Simple, down to the southeast faults match nearly as well as b) a complicated graben model. However other geophysical methods and field mapping are in agreement with the complicated graben model. Black dots represent the locations of the collected data points.**

3.3.2 Aeromagnetic survey

3.3.2.1 Survey parameters

The following summary is an excerpt from the Edcon-PRJ report submitted to Ormat.

Using an ultra-light aircraft, a high-resolution aeromagnetic survey was carried out over Ormat Nevada's Glass Buttes project area in Oregon.

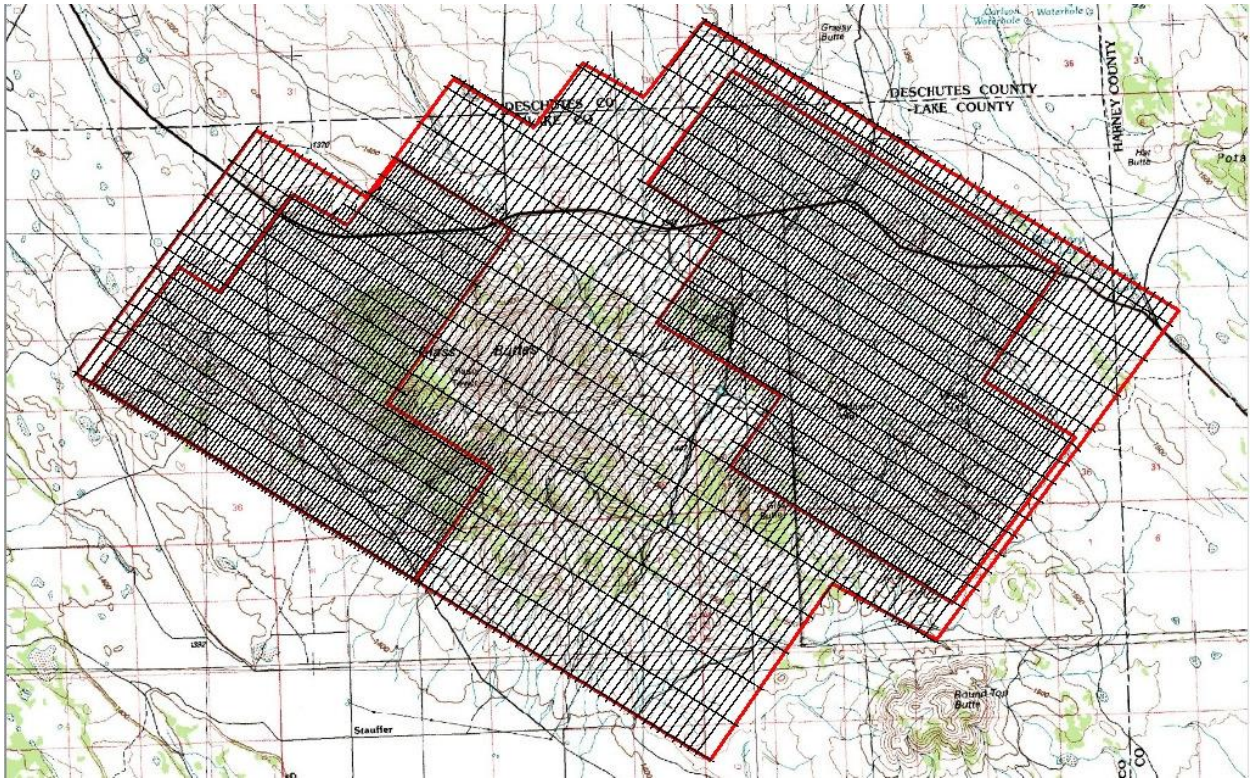

Figure 16. Aeromagnetic survey location Maps – Survey Line Locations

Northeast-southwest primary survey lines were spaced at 200-meter intervals with northwest-southeast tie-lines spaced at 1000 meters. In the southwest and northeast corner two additional areas inside the main survey were flown with line spacing at exactly half of the original line spacing. Average terrain clearance was 223 meters from the sensor. A total of 1352 line-miles of aeromagnetic data were acquired. Survey operations were completed on May 25, 2010.

Processed survey data including a total magnetic intensity map were transmitted to Ormat Nevada Inc. on May 27, 2010. Processed data also included Horizontal Gradient, Tilt Derivative, and Horizontal Gradient of Tilt Derivative maps. Horizontal gradient maps show where there is the greatest change in the magnetic field and can be useful for indicating fault locations when two units of differing magnetic susceptibility are placed adjacent to each other through faulting. Tilt derivative is the inverse tangent of the vertical derivative divided by the horizontal gradient magnitude, and acts as an automatic gain control and makes it easier to see low amplitude lineations. The horizontal gradient magnitude of the tilt derivative defines the edges of low amplitude features.

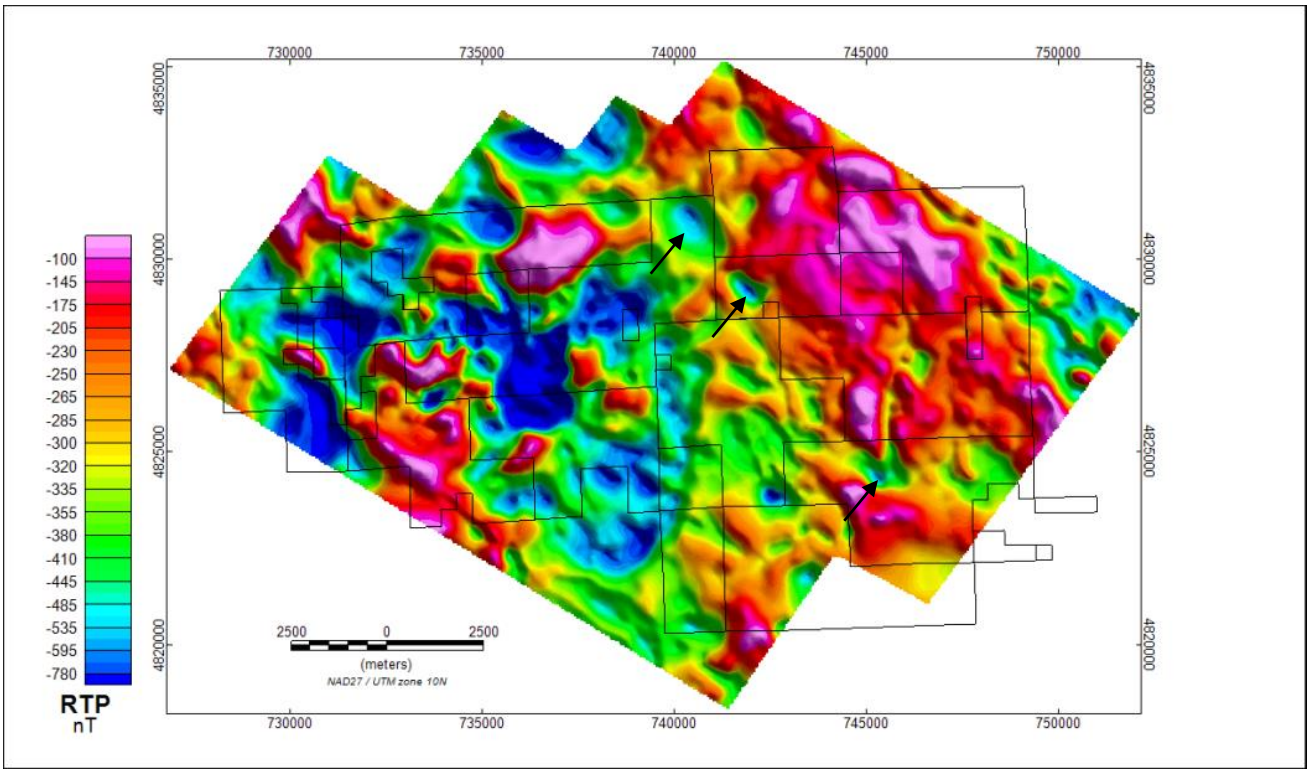

Figure 17. Aeromagnetic data reduced to pole (RTP) map in NAD 27 with arrows pointing to volcanic vents.

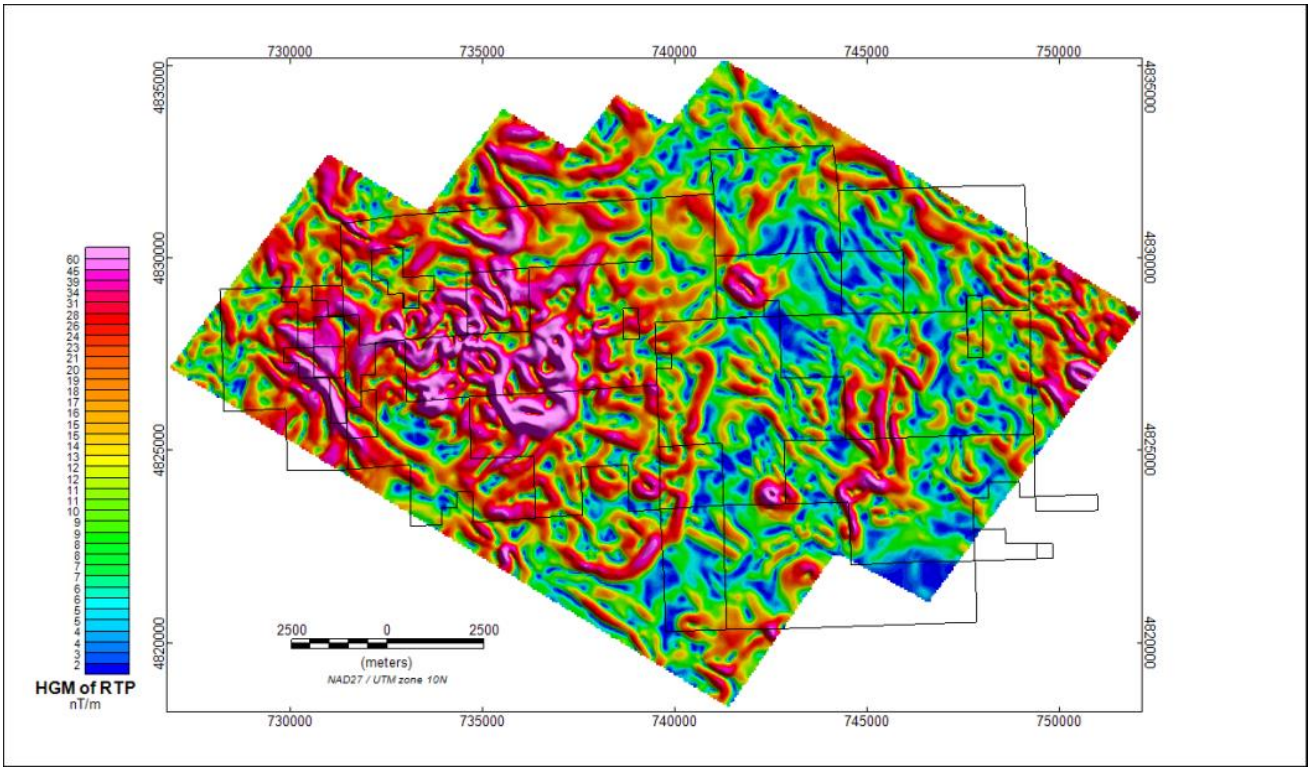

Figure 18. Horizontal gradient of reduced to pole aeromagnetic data calculated from Figure 17.

3.3.2.2 Survey interpretation

Abrupt changes in Reduced to Pole (RTP) or Tilt Derivative magnetic data may indicate lateral changes in rock type or alteration intensity. Where linear, these abrupt changes are likely to indicate faulting where different rock types are juxtaposed. Where curvilinear or circular, these changes may indicate volcanic sources or localized alteration. Hydrothermal alteration transforms magnetic minerals to hydrous oxide minerals and, and clays may replace other minerals (Glassley, 2010). Both of these have the effect of reducing the rock's magnetic susceptibility, and results in a low magnetic anomaly. Magnetic Susceptibility is a rock property that indicates the degree of magnetization of a material in response to an applied magnetic field. In this case the applied magnetic field is the Earth's magnetic field and rocks containing a lot of magnetite such as basalt would have a high magnetic susceptibility and result in the measurement of a high total magnetic field. So we are assuming that low magnetic field measurements are related to destruction of magnetite by hydrothermal alteration resulting in a lowering of the magnetic susceptibility. The shapes derived from the modeling and the actual magnetic susceptibility values are still non-unique.

Linear features are very common in the RTP data (Figure 19); in some cases fractures correspond exactly with fractures at the surface and in other cases likely indicated buried fractures in the subsurface. The western half of the survey has significantly lower magnetic susceptibility than the eastern half. This difference may be associated with bulk rock types and thicknesses or alterations associated with emplacement of the domes. Figure 20 and Figure 21 include a) processed data and b) interpreted data from Midnight Point and Mahogany areas, respectively. Brothers Fault Zone and Basin and Range Faults are apparent in the data and agree with those describe in the geologic interpretation and gravity data interpretation.

The hydrothermal alteration described in 3.2.2 corresponds with lower magnetic susceptibility in the Midnight Point area. Interestingly an area of stronger low magnetic susceptibility marks the intersection with the WNW and NS trending fractures, as marked by the arrow (Figure 20). This anomaly is located adjacent to a known vent and two similar magnetic lows adjacent to vents are found along a WNW trend further North (Figure 18). This anomaly may indicate additional hydrothermal alteration at depth and agrees with general lithologic logs that are available for the Phillips Strat-1 well. The WNW trending structure at this location passes through the location of the Strat-1 well and GB-18. Based on the temperatures recorded at these wells this structure may provide a conduit for geothermal fluids at depth.

Inversion of the total magnetic field data at this location was performed using the VOXI cloud computing extension in Oasis montaj. A high susceptibility basalt flow in the top 50m of the model was used as a constraint and the results show a cylindrical low magnetic susceptibility zone located adjacent to the known vent at the intersection of multiple faults (Figure 22). Initially there was concern that the magnetic low could be partly related to remnant magnetization within the quaternary basalt flow; however this basic model shows that low susceptibility values related to alteration in the lithologies below the basalt flow could explain the observed magnetic low. This fault intersection and the temperature anomaly associated with it provide support for drilling targets in this area as described in section **Error! Reference source not found.**.

The Parmele Ridge Fault and possibly a second parallel fracture are very prevalent in the southwestern portion of the Mahogany area (Figure 21). This fracture system dominates several data sets and provides a good first target for the Mahogany area. Although datasets covering the Mahogany area were included in our model, discussion of Mahogany will be excluded from the remainder of this report because we will not be pursuing drilling targets there.

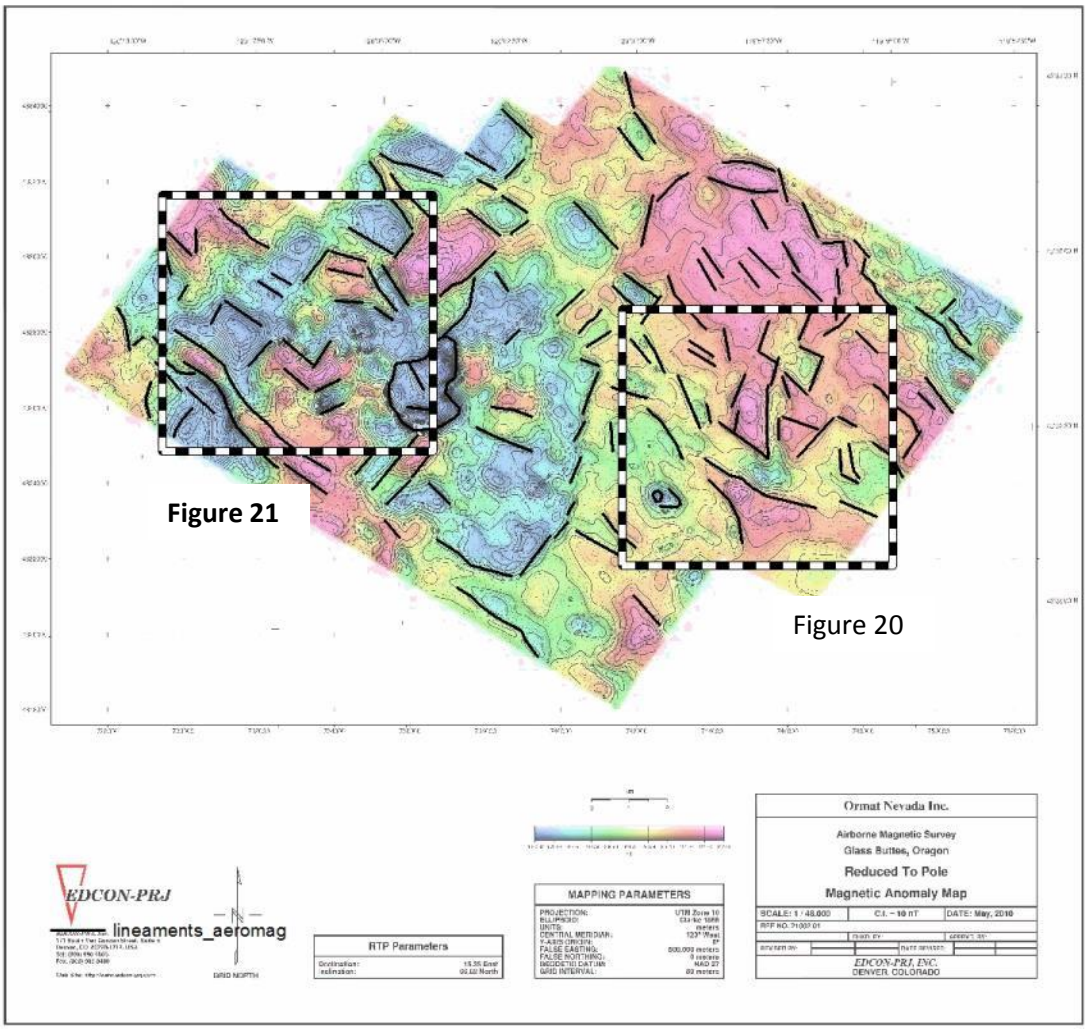

Figure 19. Interpreted Reduced to Pole map. Data are the same as shown in Figure 17 with black lines for interpreted features. Most features are faults with the exception of the circular features which are likely indicative of volcanic sources.

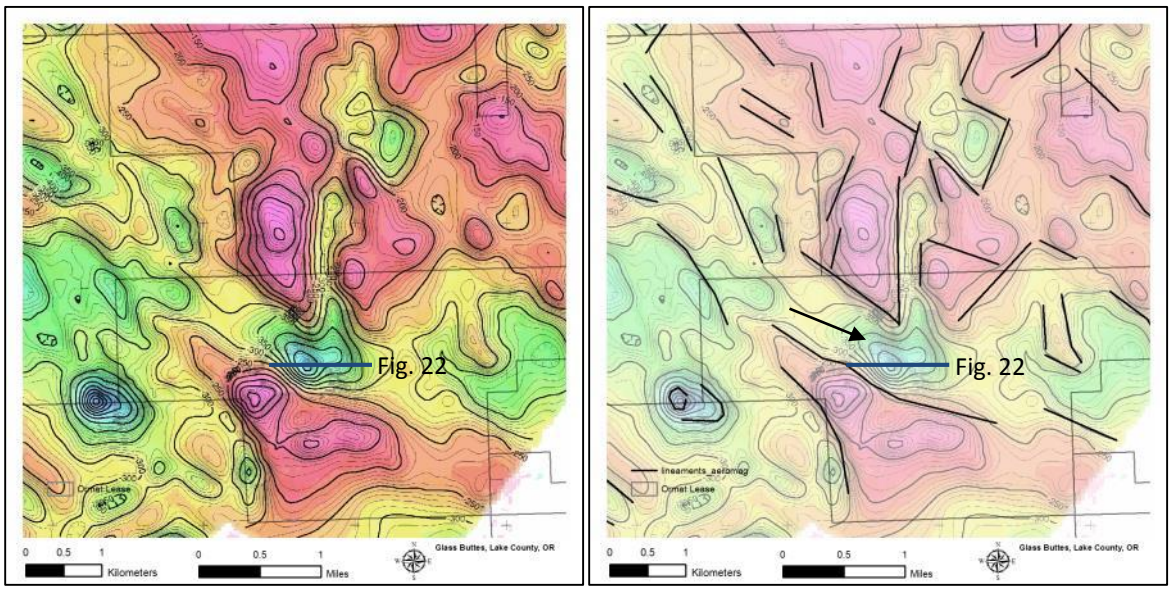

Figure 20. a) RTP map of Midnight Point area and b) the same data with interpretation. Black lines show interpreted fractures, gray lines indicate lease boundaries for comparison with other figures, and purple line shows location of cross-section for Figure 22. Scale bars are the same as Figure 19.

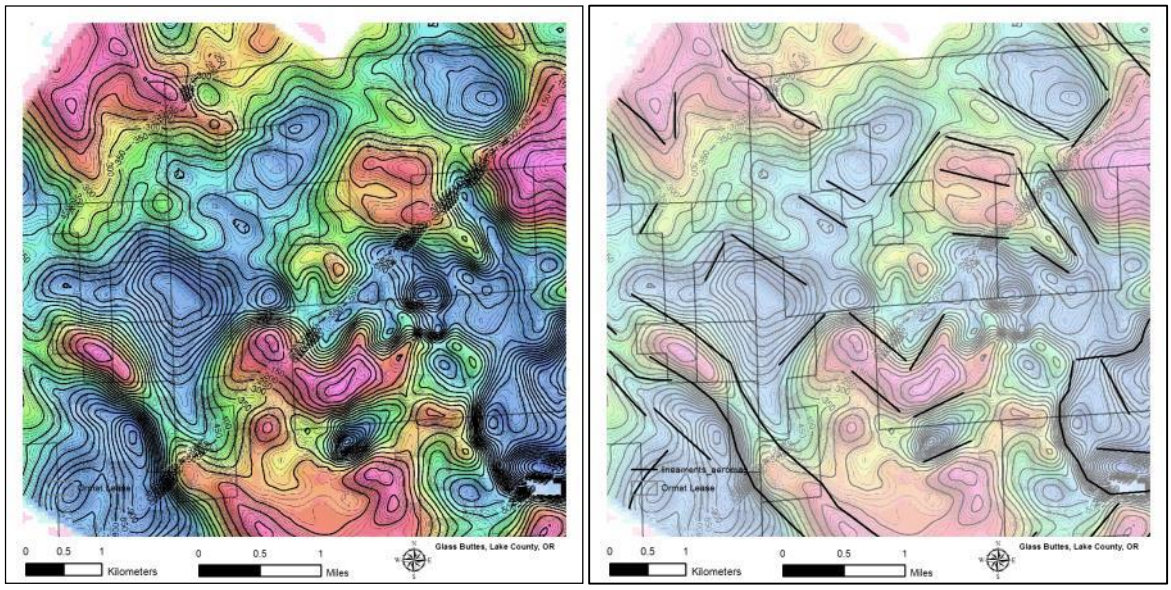

Figure 21. a) RTP map of Mahogany area and b) the same data with interpretation. Lines show interpreted fractures; gray lines indicate lease boundaries for comparison with other figures. Scale bars are the same as Figure 19.

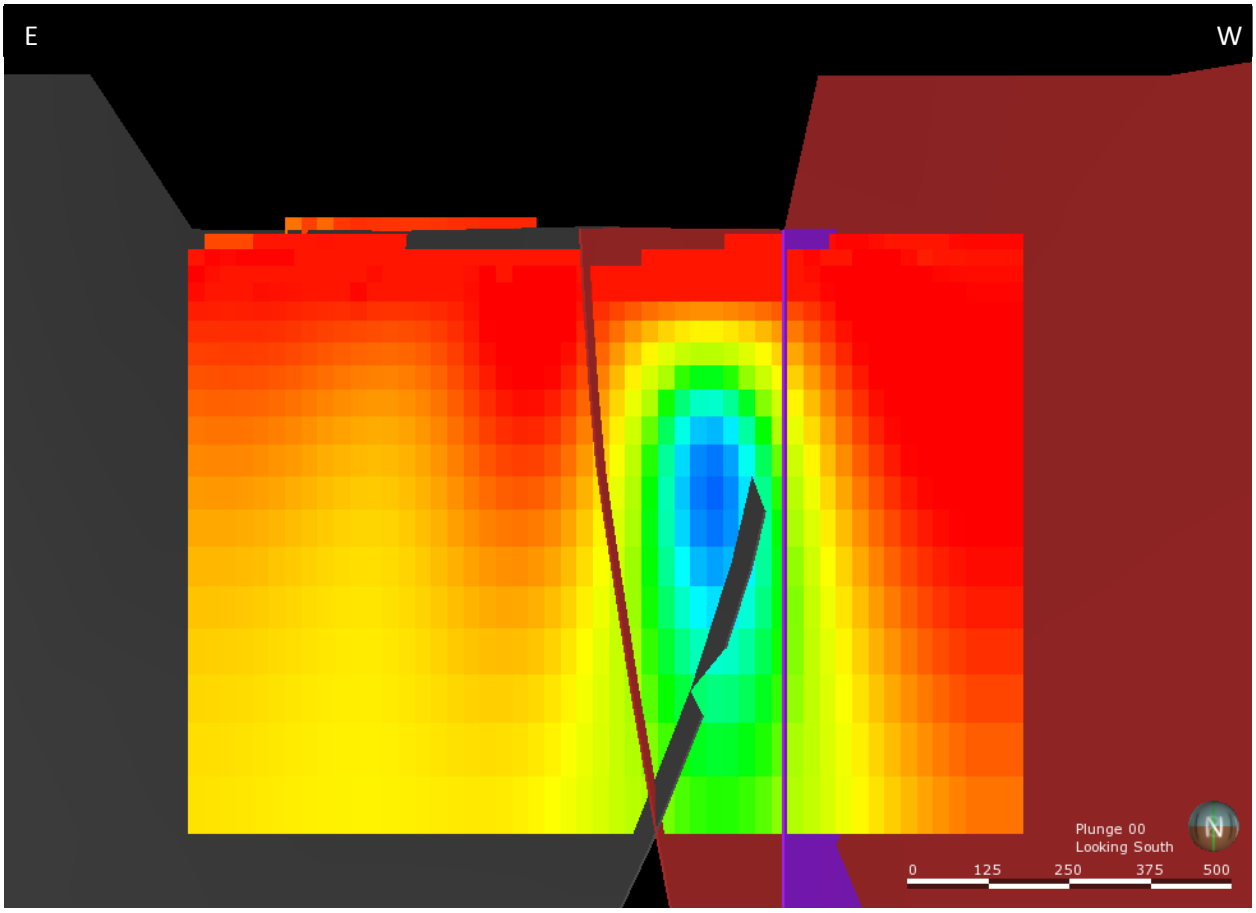

Figure 22. Magnetic susceptibility inversion of the magnetic low identified in the Midnight Point area using VOXI Earth Modeling. Cross-section is looking south at fault plane intersection.

3.3.3 Magnetotelluric

Ormat contracted Zonge Geosciences to collect Magnetotelluric (MT) data covering approximately 6000 acres over the Midnight Point area and a single line 6.7 km line across Mahogany site. The following is an excerpt from their report to Ormat with additions concerning interpretation.

This survey was conducted during the period of 7 October 2010 to 8 November 2010 and is covered under Zonge job number 2010.181. The survey area is located in T23S, R21-23E and lies within the Glass Butte and Hat Butte, Oregon 1:24,000 topographic sheets. Tensor MT data were acquired at 30 stations in the eastern survey area and Array MT data were acquired along one line, 6.8 kilometers in length in the western survey area. First a discussion on the results of the eastern area is presented followed by a discussion on the line acquired in the western area.

MT station locations for the eastern area are shown in Figure 23. Also shown on Figure 23 are the traces of two resistivity-depth sections created from 1D inversion of the static-corrected tensor determinant data.

The MT impedance tensor at each station was processed to produce the rotationally-invariant determinant resistivity and phase at each frequency. The determinant resistivity curves were static corrected using Transient Electromagnetic (TEM) data that were acquired at each station.

The determinant apparent resistivity and phase combine impedance tensor elements into single apparent resistivity and impedance phase values. The static-corrected determinant resistivity and phase data were then inverted for a one-dimensional smoothly-varying resistivity structure. It is important to note that while, these are presented in 2D or 3D views, these are 1D inversion results. Ranganayaki (1984) concluded that determinant resistivity and impedance phase were the best summary parameters to use for one-dimensional, layered-earth modeling in areas with complex two- and three-dimensional geology, in the absence of more sophisticated inversion algorithms or sufficient data density. It is also important to keep in mind when looking at these sections that the method is sensitive to conductance, which is the product of conductivity and thickness. Therefor measured responses can be explained by changes in layer thickness, changes in resistivity or both. In surveys with low data density this can make it difficult to determine the orientation of structures and it can only be concluded that there is likely a structure where there is a significant change in the response.

Figure 24 and Figure 25 show depth sections of the inversion resistivity for sections 1 and 2, respectively. The results for both sections are similar and define a 3-layer geoelectric section comprising an upper high-resistivity layer (Unit 1) that averages approximately 500 ohm-meters and is approximately 300-350m thick, a middle layer (Unit 2) of less than 5 to 15 ohm-meters that varies from 500 to 800 meters thick, and a deeper high-resistivity layer (Unit 3) of 100 + ohm-meters. Comparison with drilling results in the Strat-1 and Strat-2 holes that are located within the survey, suggest that the high-resistivity surface layer corresponds to basalt flows and relatively unaltered rhyolite. The low-resistivity unit corresponds to moderate to strong alteration within the rhyolite. It is unclear whether the higher-resistivity basal unit (3) at depths of estimated at approximately 600 to 650m below surface near the Strat-1 well, has been tested. This depth is very close to the TD of Strat-1.

Unit 2 is thinner, and the high-resistivity Unit 3 is shallower along the eastern side of the survey area. Marked resistivity gradients are associated with apparently thicker and lower resistivity within Unit 2 to the west and suggest probably high-angle faults.

On section 1 (Figure 24) there is a marked gradient at depth between stations 28 and 27. The Strat-1 well lies approximately 850 m to the north of station 28. The depth to the top of Unit 3 is estimated at 800 m below surface to the east of this feature, and 1000m below surface to the west. Note that there is a marked decrease in the resistivity to the west of this feature, within Unit 2, and the eastern limit of rock of less than 10 ohm-m occurs at this structure. This is evidence for a significant high-angle structure. Another resistivity gradient, suggesting a possible fault is located beneath the vicinity of station 23. Depth to Unit 3 increases to 1200m below surface to the west of this feature. This would indicate a dip down towards the northwest; however geological mapping and gravity interpretation are consistent with a southeast dipping structure at this location. The measured electrical response at station 23 could be explained solely by a decrease in resistivity towards the west related to lithology or alteration rather than a change in layer thickness; this reflects the non-uniqueness of the inversion results.

Figure 25 shows Section 2 which lies along the northern edge of the survey area and lies near a sub-parallel gravity profile. This section is similar to Section 1. A resistivity gradient is indicated between stations 2 and 7, which may be associated with a high angle fault. The depth to the top of Unit 3 is interpreted to be approximately 750m to the east, and 1250m to the west of this feature. Tipper and impedance phase data support the existence of this feature and indicate a northerly strike. This is also coincident with a pronounced gravity gradient, with increasing

gravity to the west. Note that a decrease in resistivity within Unit 2 is observed near this feature for station 3. Based on the DEM, location of the gravity gradient and MT results this fault is likely to be located between stations 3 and 7. Geological mapping and gravity data are consistent with an east dipping structure; whereas the apparent offset in the MT results indicate a western dip direction. This is likely the same structure that was identified in the vicinity of station 23 and the apparent change in the thickness of layer 2 could be explained by a decrease in resistivity towards the west related to lithology or alteration. Resistivity gradients suggesting high angle faults were also identified between stations 7 and 8, as well as between stations 9 and 14. The location of these gradients is in agreement with features identified in the magnetic survey and surface expressions of these potential faults can also be seen in the DEM.

Figure 26 shows a contour map of the results of the 1D inversion of the determinant resistivity for an elevation of 1000m. This elevations lies near the top of the low-resistivity unit 2 and is largely mapping variations in the thickness of layer 1 and/or variations in resistivity of layer 2. There is a well-defined north-northeast resistivity gradient along the eastern side of the survey area. Also observed, is a north-northeast trending resistivity gradient between stations 3 and 7 and a pronounced northwest-trending low resistivity zone.

Figure 27 shows a contour map of the results of the 1D inversions of the determinant resistivity for an elevation of 800 meters. The sharp gradient observed between stations 27 and 28 in Section 1 is clearly shown in the southern part of the map. A pronounced low-resistivity embayment is observed in the south central portion of the grid and is centered near station 26 which is near the Strat-1 well.

shows the determinant phase for a frequency of 1 hertz. This is near the resistivity minima on the resistivity versus frequency sounding curves. This is most responsive to resistivity and thickness variations at the base of unit 2. The data support the low-resistivity embayment near the location of the Strat-1 well and the thicker section of low resistivity to the west. The impedance phase data are not susceptible to static effects.

Also shown on this plot are polar diagrams of the impedance tensor for 1 hertz. The outer curve of this plot represents the magnitude of Zxy as it is rotated through 360 degrees. The inner curve represents the magnitude of the diagonal elements Zxx. For a 1D earth the curve will be a circle. For 2D and 3D earth the curves will be elongate and the azimuth of the maximum resistivity will rotate in relationship to the location of 2D and 3D structure.

Figure 28 shows the Tipper magnitude for a frequency of 1 hertz. The Tipper is non-zero only in the presence of lateral resistivity contrasts. The Tipper is useful for determining strike direction and tracing such structures. The pronounced and relatively continuous Tipper high trending northerly through the grid indicates a significant resistivity contrast and is the dominant feature at the depth of layer 2. The western side of the Tipper peak is associated with a gradient in the Impedance phase and the gradients/faults suggested on Sections 1 and 2.

Figure 30 shows the impedance phase at 0.125 hertz. A northerly-trending high in the impedance phase suggests a low-resistivity zone and or a linear zone of greater depth extent located immediately west of the suspected fault observed on section 2. The circular phase high located in the south central "embayment" near the Strat-1 well supports a deeper-extending low resistivity zone and indicates that this feature is not related to residual static effects.

In summary, the MT survey has mapped vertical and lateral variations in resistivity that defines "layers" and can be interpreted to provide the locations of high-angle structures. The vertical layering may relate to thermal alteration products, primary lithology, groundwater content and salinity or all of the above. Drill information gives good correlation with the top of the low-resistivity Unit 2 and the top of strong alteration in the Strat-1 and Strat-2 wells. The source of the deeper, resistive Unit 3 is not recognized and while the Strat-1 well came close, it is not clear as to whether it should have intersected it.

Multiple lines of evidence indicate that a northerly-trending structural zone is a dominant feature within the survey area. A pronounced low-resistivity zone in the vicinity of the Strat-1 well is detected and may represent a zone of structural intersection. The northerly-trending low resistivity zone in this vicinity and on the west side of the survey area represents a good target for increased fracture permeability indicated by the intersection of multiple inferred faults from the DEM, gravity and magnetic surveys. Fault intersections in the vicinity of the Strat-1 well and its associated temperature anomaly will be the primary focus of drilling efforts.

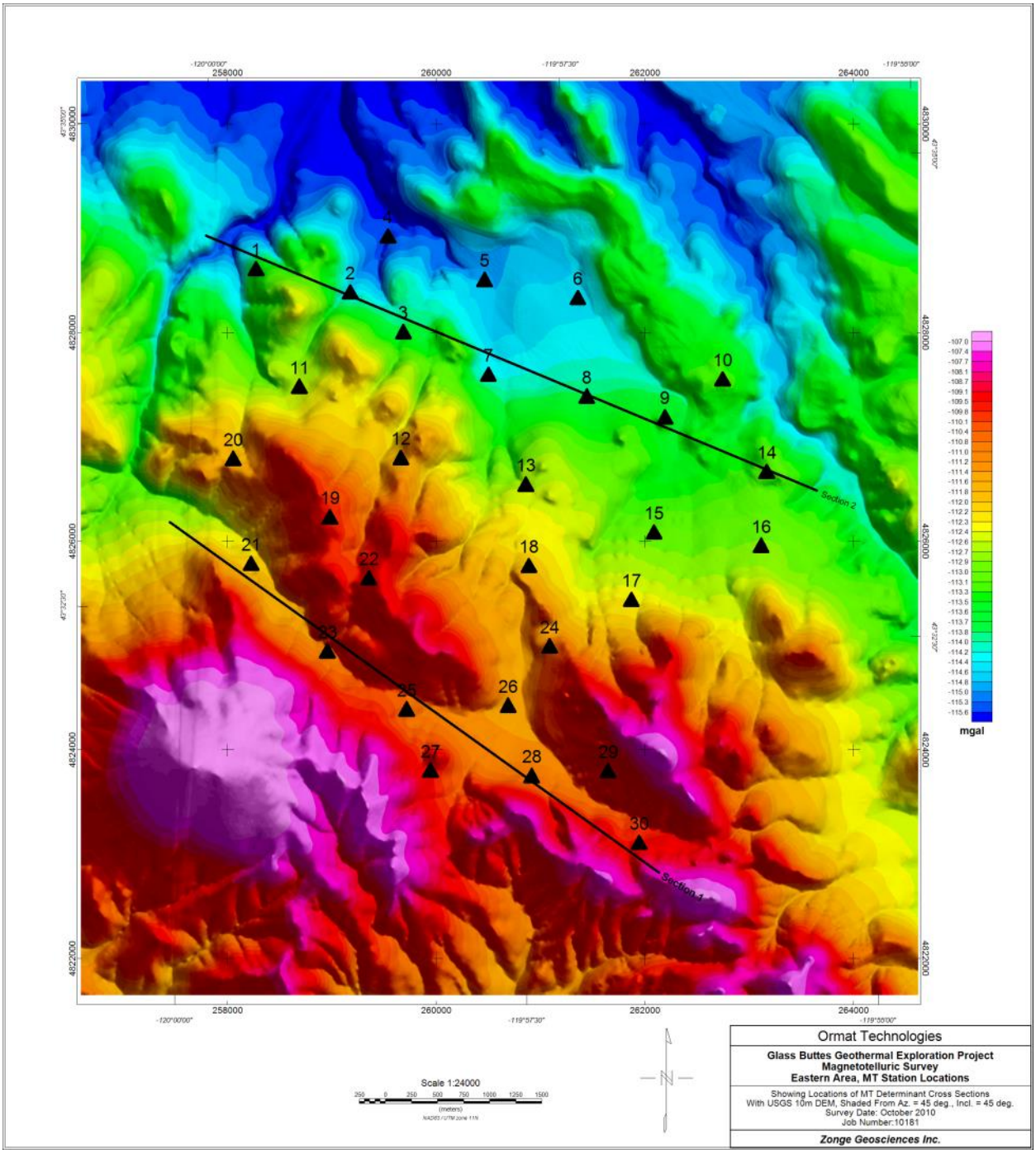

Figure 23: Map showing the location of MT stations and resistivity-depth sections presented in Figure 24 and Figure 25.

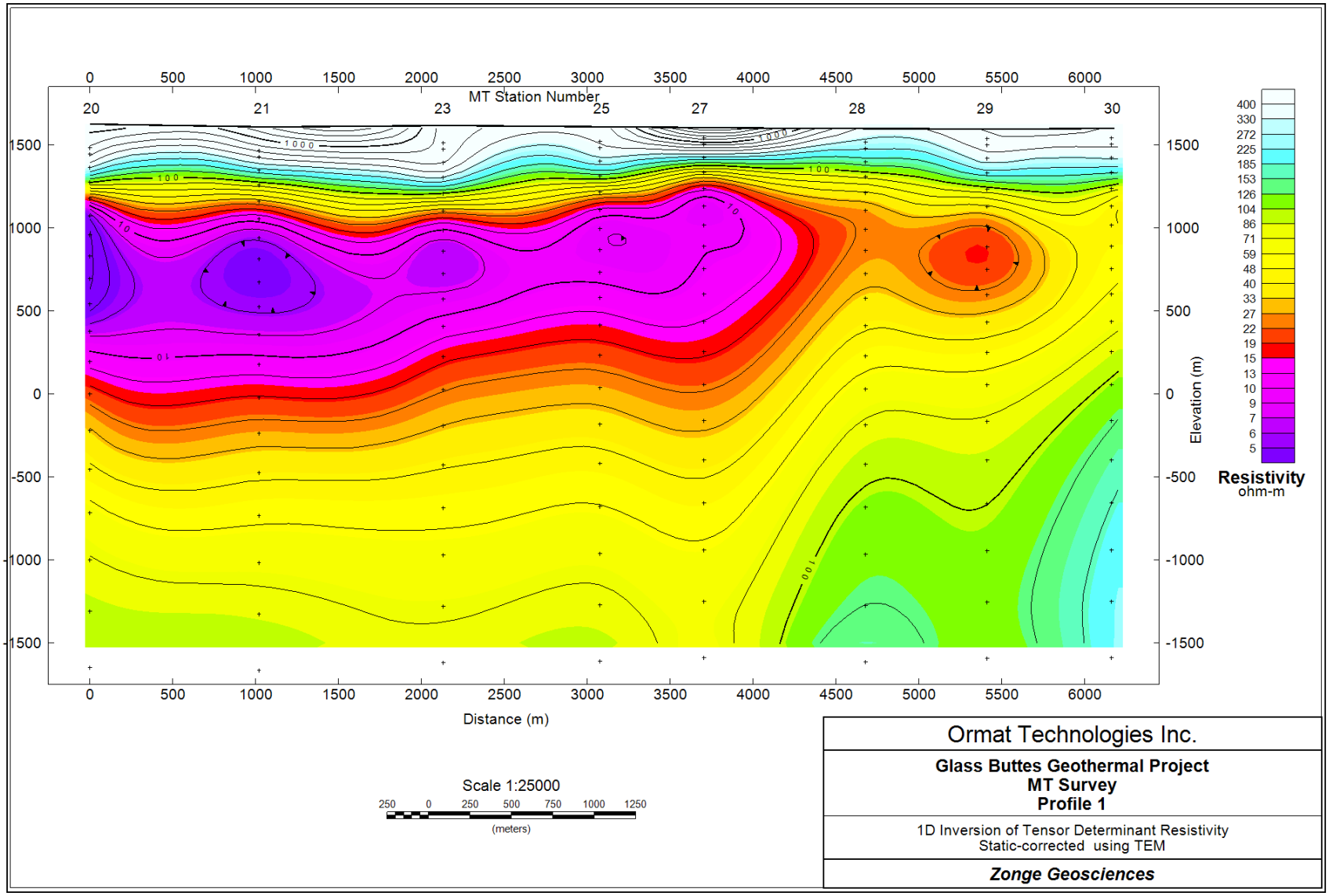

Figure 24. Inversion resistivity-depth section from one-dimensional inversion of the tensor determinant resistivity for profile 1 as shown on Figure 23.

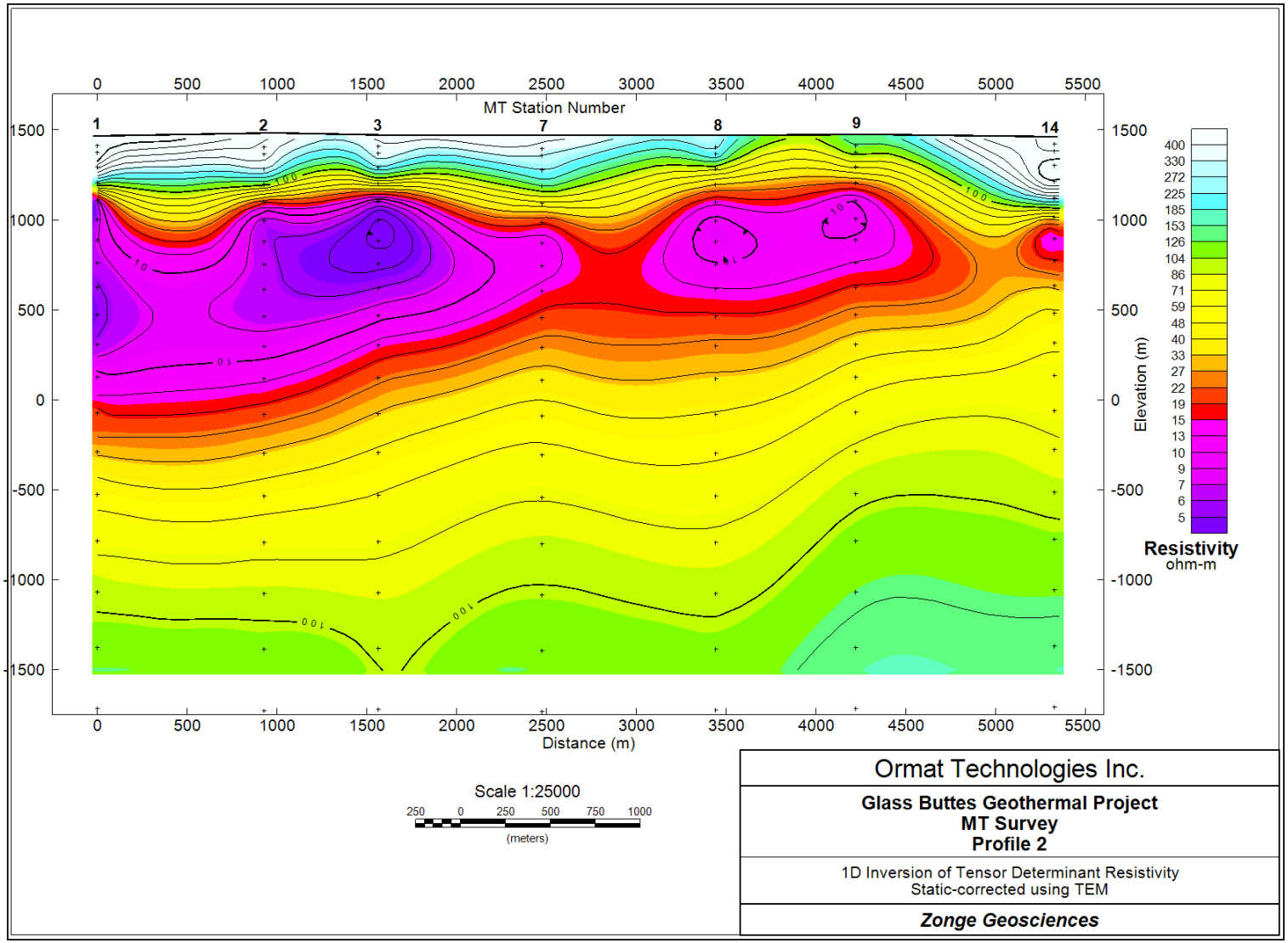

Figure 25. Inversion resistivity-depth section from one-dimensional inversion of the tensor determinant resistivity for profile 2 as shown on Figure 23.

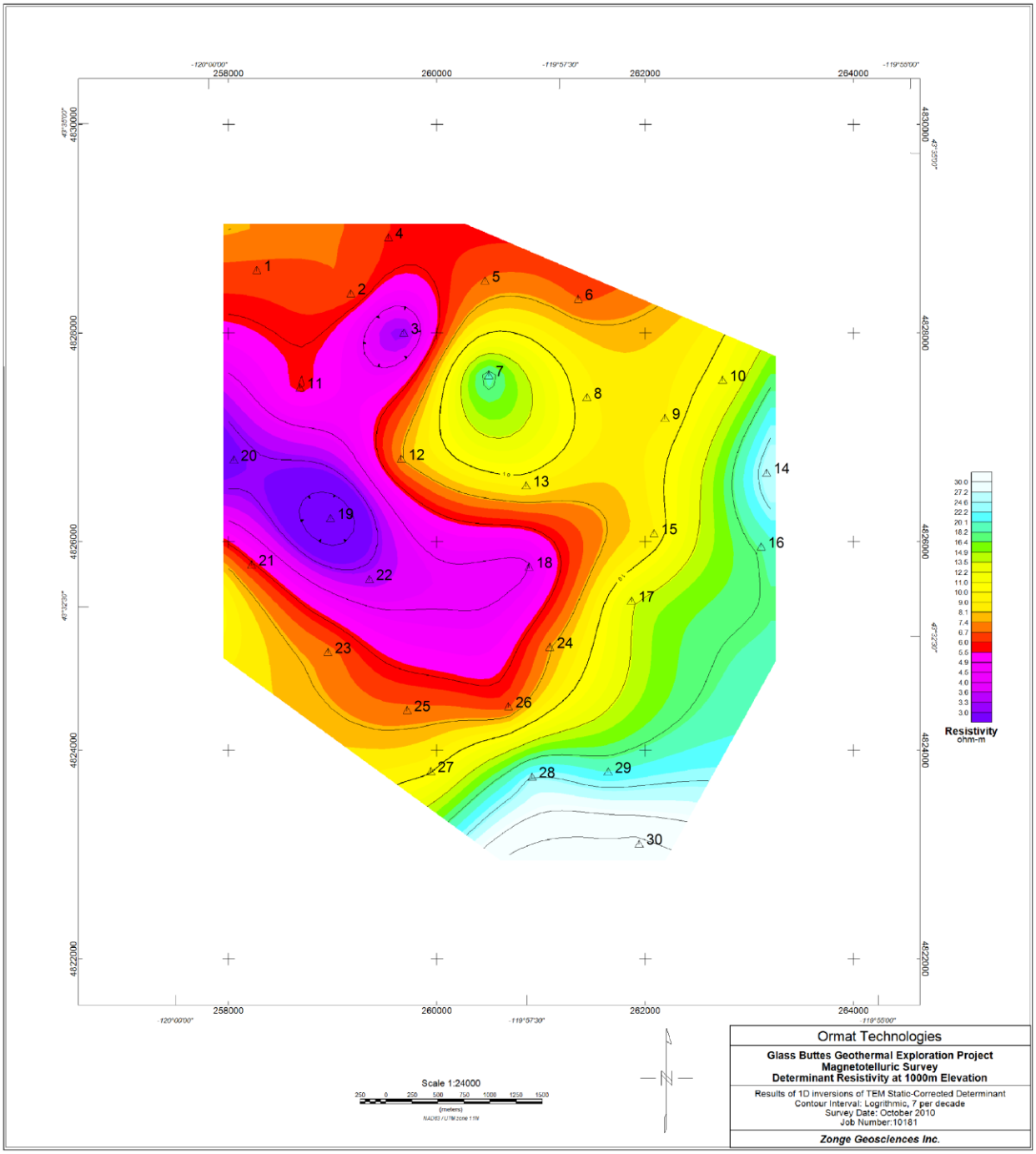

Figure 26. 1D inversion results of static-corrected determinant resistivity for an elevation of 1000m.

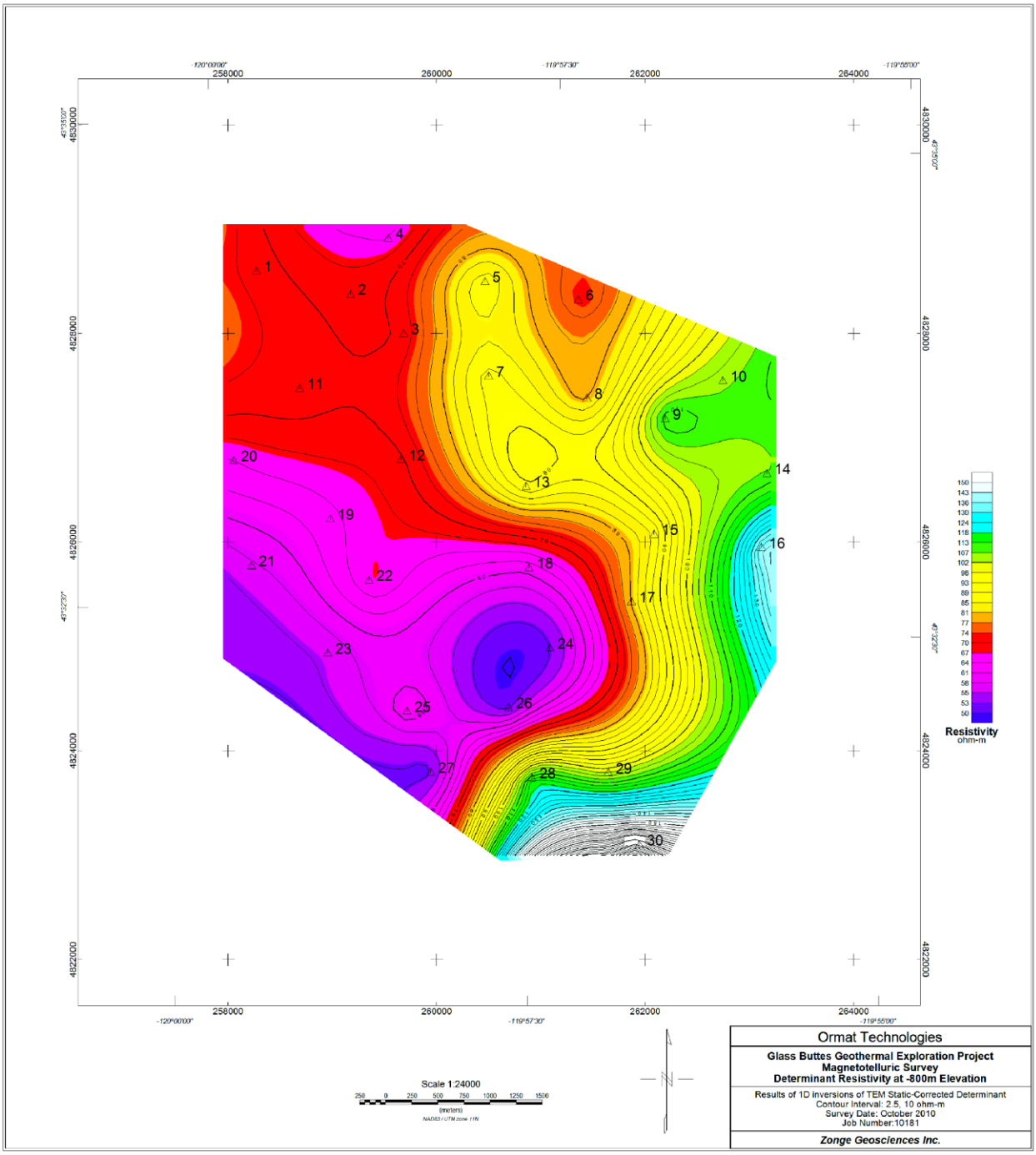

Figure 27. 1D inversion results of static-corrected determinant resistivity for an elevation of -800m.

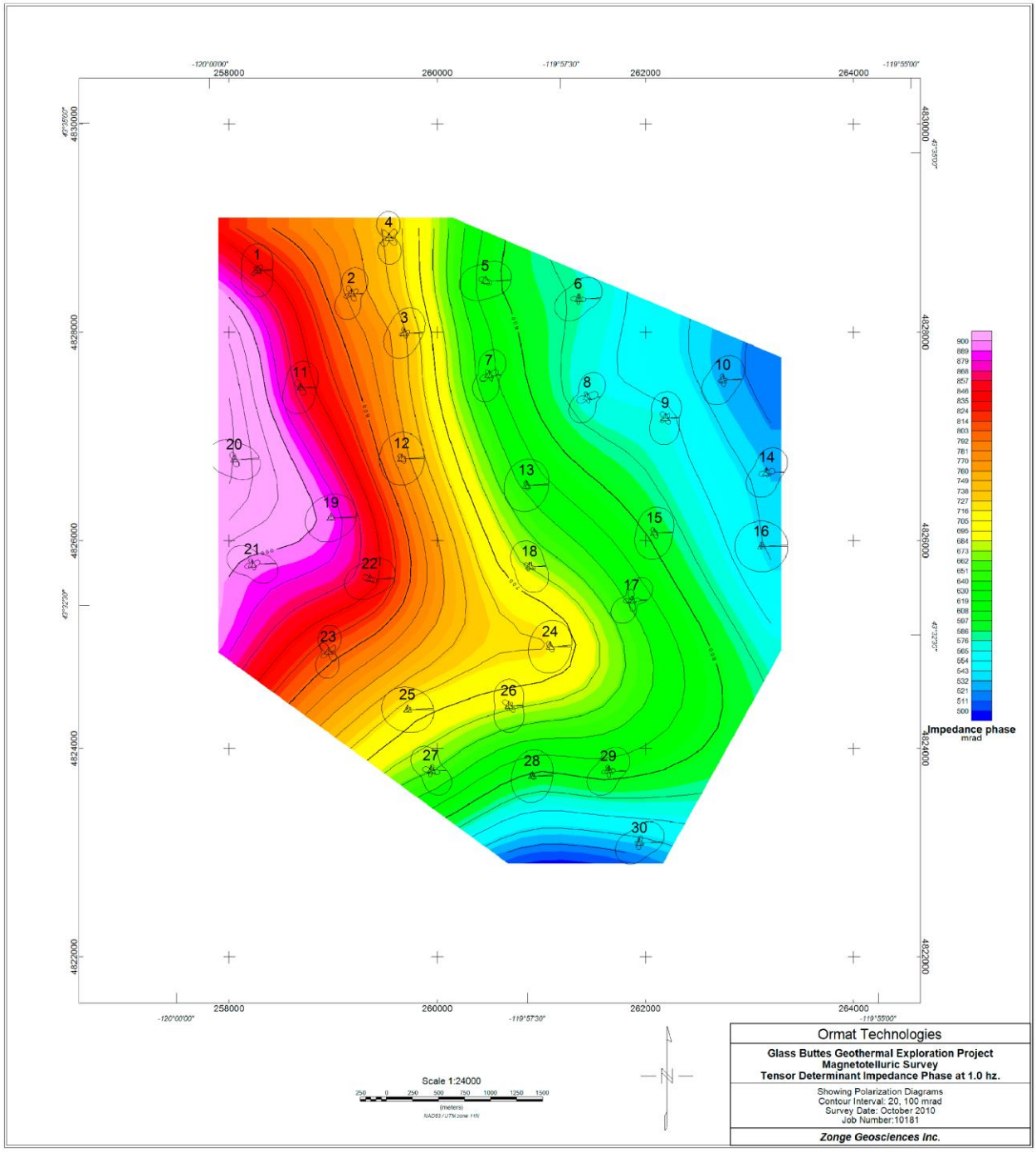

Figure 28. Contour map of the Determinant phase at 1 hertz. Also shown are polar diagrams for the impedance tensor at 1 hertz.

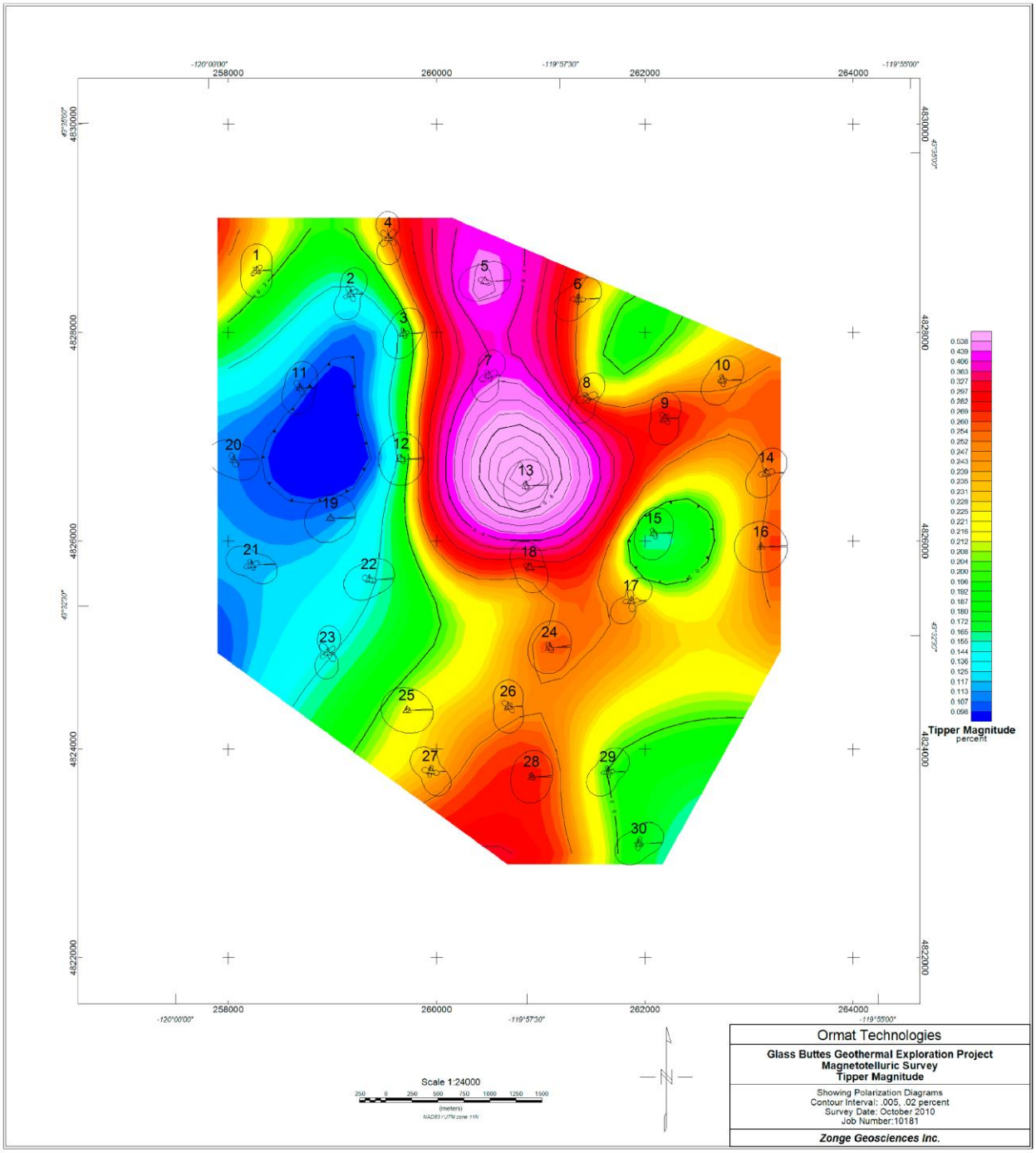

Figure 29. Contour map of the tipper magnitude at 1 hertz. Also shown are polar diagrams for the impedance tensor at 1 hertz.

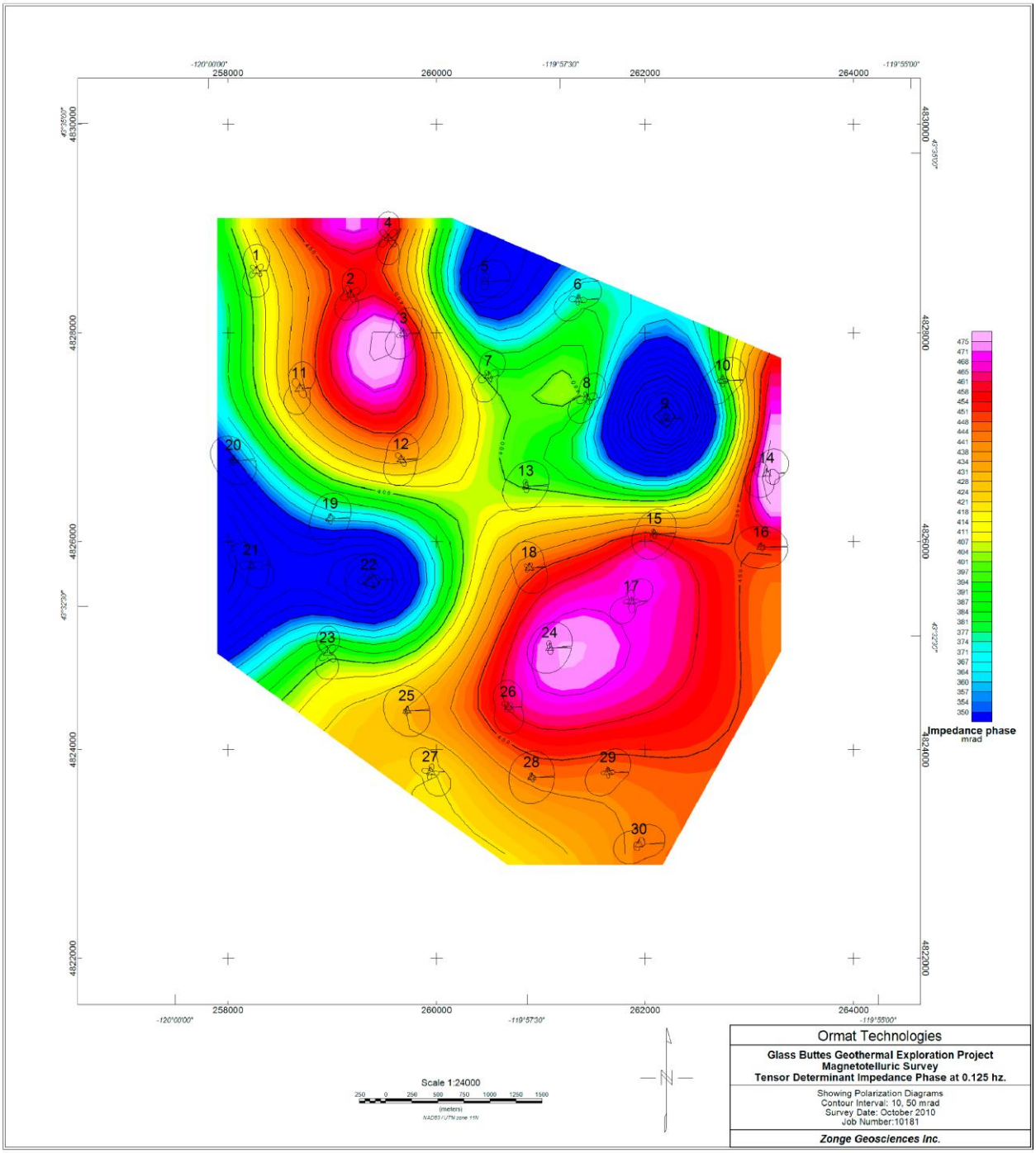

Figure 30. Contour map of the Determinant phase at 0.125 hertz. Also shown are polar diagrams for the impedance tensor at 0.125 hertz.

Figure 31 shows the MT line on the horizontal gradient of the Complete Bouguer Anomaly at the Mahogany site. This line follows a detailed gravity line that was presented earlier in section

3.3.1.2 Gravity data interpretation.

The broad, northwest-trending gravity gradient, increasing to the northeast, is observed at the northern half of the line. This gradient forms the southern edge of the broad gravity high that is observed to the north of Glass Buttes and is thought to represent a major deep-seated structure. The horizontal gradient shows several distinct gradients that are thought to be caused by offsets of the relatively shallow volcanic section. The observed orientation is more northerly than observed for surface faults, which are dominantly northwest trending in this area.

Figure 32 shows the results of the two-dimensional smooth-model inversion of the Zxy (TM-mode) tensor MT data. The results show a high-resistivity surface layer of 200 to 400 ohm-m lying at surface of covered with a thin lower resistivity soil layer. This unit is 100 to 150 feet thick and is interpreted to represent young basalt flows. A thin low-resistivity unit of 15 to 20 ohm-m and 50 to 100m thick underlies the young basalt and likely represents a sedimentary or volcaniclastic layer. A deeper layer of 75 to 100+ ohm-m lies beneath this unit and shows a marked thickening to the north of station 2400. The contact at the top of this unit with the low-resistivity shows an increase in depth of approximately 150 meters to the northeast of this location. The thicker section may be caused by deposition within a graben. Low resistivity of 10-15 ohm-meters beneath this layer may represent moderately altered rhyolite. A pronounced low resistivity unit of 2 to 5 ohm-meters is indicated at depths of approximately 750 meters beneath the southwestern end of the line and increases in depth to 900 to 1000m beneath the central portion of the line. Based on the correlation with well logs in the eastern area, this could be intensely-altered rhyolite. An increase in resistivity is observed at depth beneath the entire line and this unit forms the effective electrical basement for this survey. The top of this unit lies at a depth of approximately 1200m beneath the southeastern end of the line and approximately 1700m beneath station 5300. The depth to this unit decreases to approximately 1400m beneath the northeastern end of the line. The general structure, interpreted from the 2D inversion results is a graben beneath the northern two-thirds of the line, which agrees with surface geologic mapping. The deepest portion of the graben lies beneath stations 4800 to 5900. To the southwest of this location the volcanic stratigraphy appears offset on faults that are down to the

northeast, with gentle tilting of blocks to the southwest. In the northeast near station 5900 the units appear to be offset down to the southwest. The northwestern end of the line straddles the broad gravity gradient. This is thought to represent the southern boundary of a deep, high density block and is thought to be a deep-seated structure controlling the location of Glass Buttes.

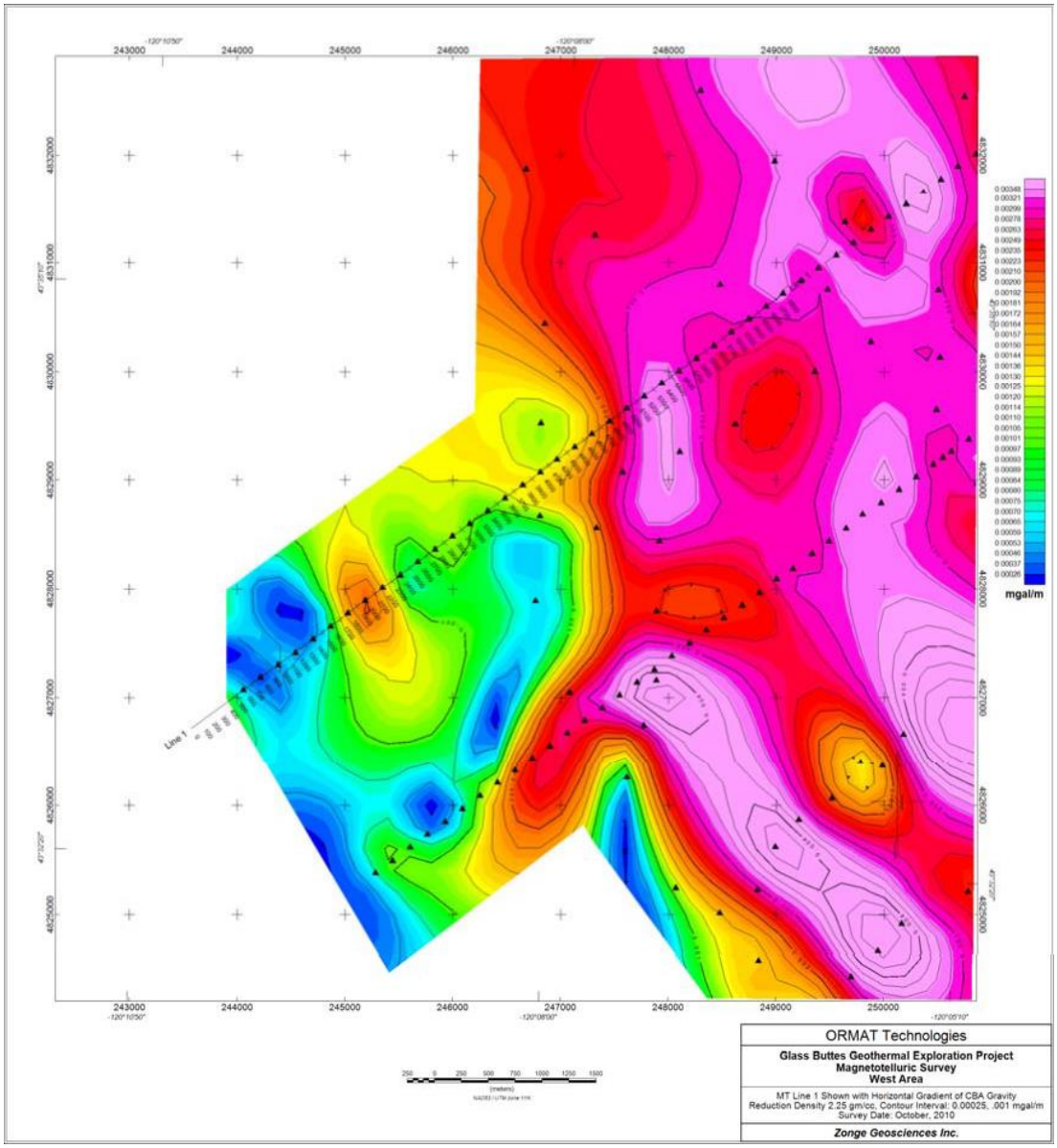

Figure 31. MT stations acquired over a detailed line at the Mahogany site shown with the horizontal gradient of the Complete Bouguer Anomaly.

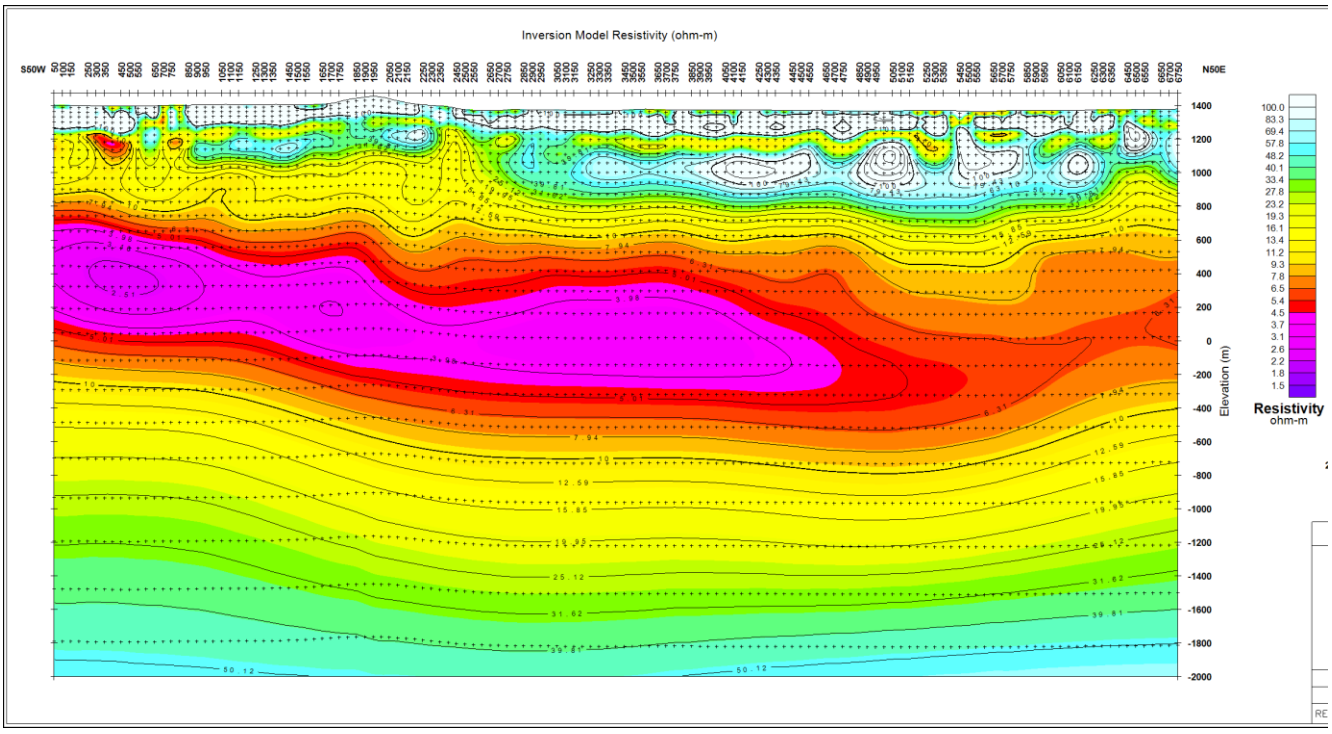

Figure 32. Two-dimensional smooth-model inversion of the Zxy (TM- mode) tensor MT line acquired at the Mahogany site.

4.0 Integrated analysis of results and conceptual resource model

Ormat used Leapfrog 3D software to incorporate all geological and geophysical data sets into a comprehensive model (Figures 33-35). We created three dimensional curvilinear fault planes to honor interpretations from all data sets. We inferred subsurface lithologies from records of previously drilled wells, but our understanding of lithologic contacts and alteration assemblages will be greatly improved with future drilling. These fault planes provide drilling targets that are anticipated to provide enhanced permeability for high temperature fluid flow as described in section **Error! Reference source not found.**. The value of the resulting model is impossible to illustrate in 2 dimensional figures, and a short movie is included with this report to illustrate the complexity of the model and some of the drilling targets that were proposed. Each well that Ormat drills will be used to revise and better constrain the model, further reducing risk for future wells.

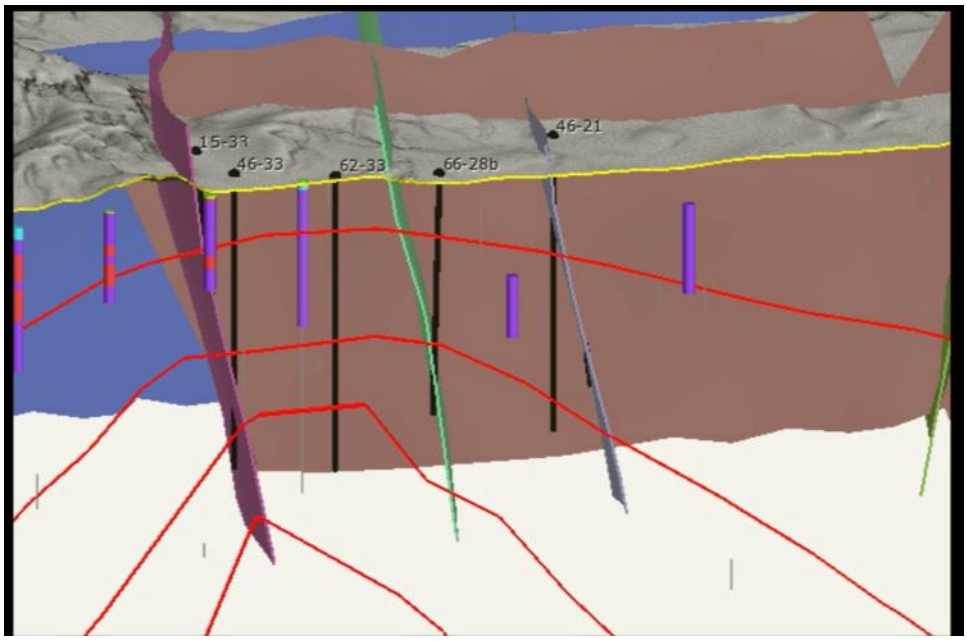

Figure 33. Screen capture looking west northwest through model section with previously-drilled wells (colored bars) and proposed wells (black, labeled bars). Colored planes represent faults, red lines temperature contours in 50 C increements from 50 to 200 C. Note that these temperatures are based on gradient projections because well control only reaches 93 C.

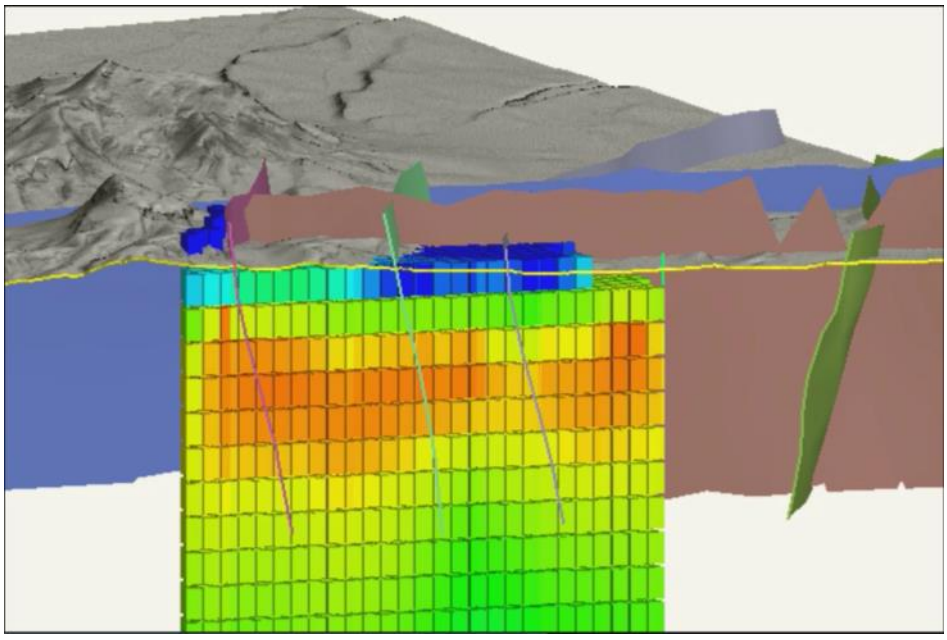

Figure 34. Model section looking west northwest, zoomed out from Figure 33, with colored boxes indicating low (red) to high (blue) resistivity in MT data. Colored boxes are voxels from extrapolation of 1D MT inversion.

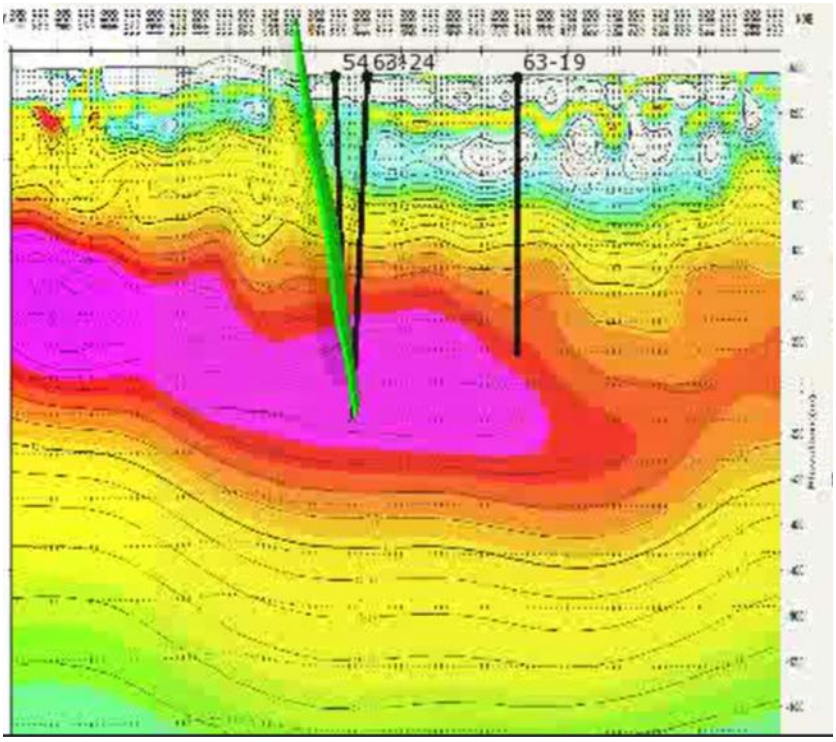

Figure 35. Mahogany area model section looking northwest along Parmele Ridge Fault with possible future wells (black bars).

Many of the structures identified by detailed geological mapping can be clearly seen in the magnetic data. Figure 36 shows the reduced to pole magnetic anomaly map along with mapped structures and MT stations. In order to explain the geophysical data two additional structures (blue) must be added to the geological model. The NE trending structure on the east side of the map can be identified in the DEM and appears to be an extension of the NE trending structure located to the north of it. This structure was mapped dipping down towards the NW in the northern end of the map, which is in agreement with the high angle structure identified by MT profile 1 between stations 27 and 28 at the southern end of the map. This structure can also be seen in MT profile 2 between stations 9 and 14. The N-S oriented structure that is interpreted from the magnetic survey follows a creek bed along half of its length to the north in the vicinity of GB-22. This structure can be seen in MT profile 2 between stations 7 and 8 where there is a significant resistivity contrast. The two geophysically-defined structures form a graben that narrows southward. Both may provide additional fracture permeability in the highest priority area in the vicinity of the Strat-1 well.

The gravity data does not match the faults mapped at the surface as closely as the magnetic data. The gravity signal is more representative of deep seated basement structures and many of the

faults mapped at surface are cross-cutting volcanic units where there is perhaps not a significant density contrast. The structures identified by geologic mapping and interpretation of the magnetic and MT data coincide with or appear as discontinuities in the horizontal gradient magnitude of the Bouguer gravity map (Figure 37). Two of the NE trending faults from the geological map are visible in the center of the horizontal gradient map shown as dashed lines in Figure 37. It is important to note that the maximum horizontal gradient is located above where the fault plane occurs at depth. The location of these maxima SE of the surface expression of the faults is consistent with a dip down towards the SE stepping into graben structure as shown in Figure 15B. The more extensive NE structure that continues SW across the geological map correlates with resistivity contrasts between stations 3 and 7 in MT profile 2 and in the vicinity of station 23 in MT profile 1. A third linear feature in the horizontal gradient of the complete Bouguer gravity map located directly southeast of these mapped faults may represent an additional deep seated structure trending NE, which is consistent with the model in Figure 15B. The NE trending and NW dipping geophysically-defined structure (solid blue line) discussed earlier forms the opposing graben bounding fault.

Additional quantitative analysis and geophysical data acquisition could improve our understanding of the geology, especially following density and magnetic susceptibility measurements of core collected during the drilling campaign. Numerical modeling of the aeromagnetic and gravity data could be undertaken to help quantify the thickness of individual extrusive flows and igneous intrusions, as well as improve our understanding of the fault geometry. The resistivity model determined by one dimensional inversion of the MT stations at Midnight Point does not provide sufficient resolution for a detailed analysis of the structures present at this location. Additionally, the large station spacing precludes 2D or 3D inversion. If subsequent geophysical work is warranted based on phase I drilling results, detailed MT lines should be completed over the most important structures with two dimensional inversions to gain a better understanding of the fault geometry at depth.

5.0 Well Targeting

Indications of temperature are prevalent at Glass Buttes. Temperature anomalies interpreted from Phillips drilling in the late 1970s total 60 km^2 (23 mi^2) of temperature gradients over 165° C/km (10° F/100ft). Deeper drilling by Phillips at Midnight Point included Strat-1, which reached a temperature of nearly 90°C (194 °F) at 603 m (1981 ft), with an impressive bottom-hole gradient of 165° C/km (10°F/100ft). Located to the northwest of Strat-1, the shallower GB-18 displayed a

higher gradient – if they were to maintain this gradient both wells would reach a temperature of 150°C at a depth of only 914 m (3000').

Ormat's conceptual model is that fluids flow up along the NW-striking fault that connects GB-18 and Strat 1 and this fault's intersection with NNE-striking faults. The high shallow gradients to the north are a result of outflow along faults with both orientations. This hypothesis is supported by 1) the magnetic low along the north-trending graben 2) the low resistivity along these structures at depth, and 3) the rapid decline in temperature gradient to the south.

Permeability is more unknown at Glass Buttes and the identification of structures to provide it was the main focus of the studies outlined in this report. None of the historic drilling tested for permeability, but circulation losses were common. In addition, those wells were drilled without a clear structural model. We hope that our extensive work identifying structures will assist in drilling into permeable zones.

Our proposed wells were sited to target faults near where temperature is elevated and alteration is abundant. The innovative exploration program has been invaluable for identifying these fault structures, and combined with high temperature zones identified in the historic drilling we have been able to site a number of exploration wells. The structures around Strat-1 are of highest priority for future drilling, due to 1) the elevated temperature gradient measured in that well, and 2) the proximity to structural intersections. Structural mapping by Boschmann (2012) in the field and using LiDAR, as wells as the gravity and magnetics data identified a northwest-trending structure that appears to run between Strat-1 and GB-18. This structure trends similar to the greater fabric of the Brothers Fault Zone and may provide a conduit for the geothermal reservoir indicated by the temperatures seen in Strat-1 and GB-18.

Our 52-33 well targeted this structure and its intersection with geophysically defined structures with nearly perpendicular orientations. We proposed this as our first well to test the resource at Glass Buttes. Field observations of structures with a similar orientation to the NW trending structure have a dip of 66 degrees in this area. Assuming a fault dip between 65 and 70 degrees, we expected 52-33 to intersect the structure at a depth of between 2700 and 3500 feet (figure 43). The dip of the NE trending geophysically defined structure is poorly constrained; however with a dip of roughly 75 degrees it would be encountered at the targeted intersection with the NW trending structure (Figure 44). The well was planned to be drilled to 3000-4000 ft. depth, pending temperature and permeability results while drilling. The next likely targets were along the Cascade Fault, the next fault to the south, to explore the potential along that similarly-trending system that also has hydrothermal alteration along it.

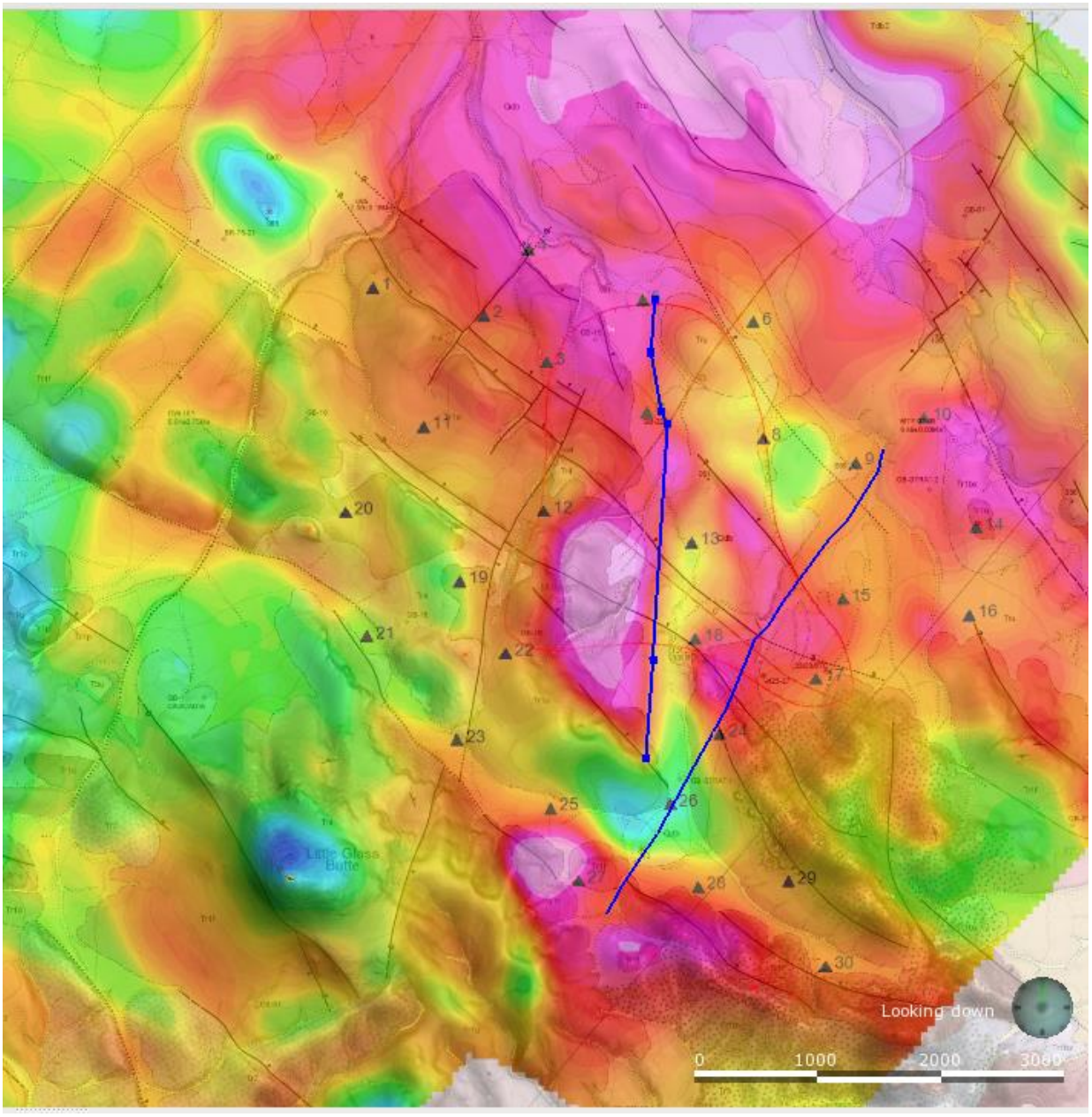

Figure 36, Reduced to pole magnetic anomaly map with mapped structures and MT stations in the Midnight Point area. Blue lines are interpreted structures from geophysics that are not observed in surface geologic mapping.

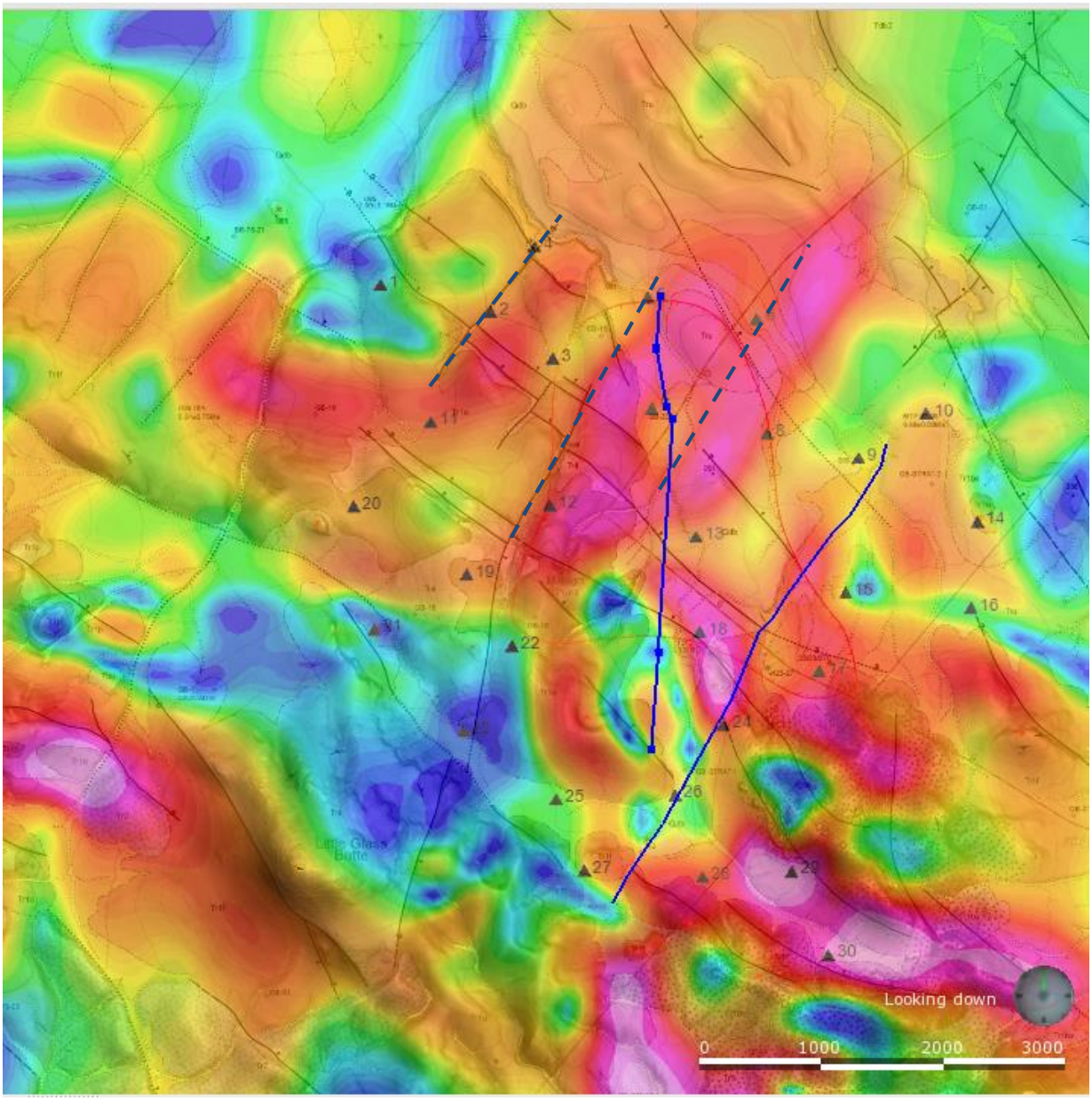

Figure 37. Horizontal gradient magnitude of the complete Bouguer gravity with mapped structures and MT stations in the Midnight Point area. Dashed lines highlight NE trending faults stepping down towards the SE into a graben structure

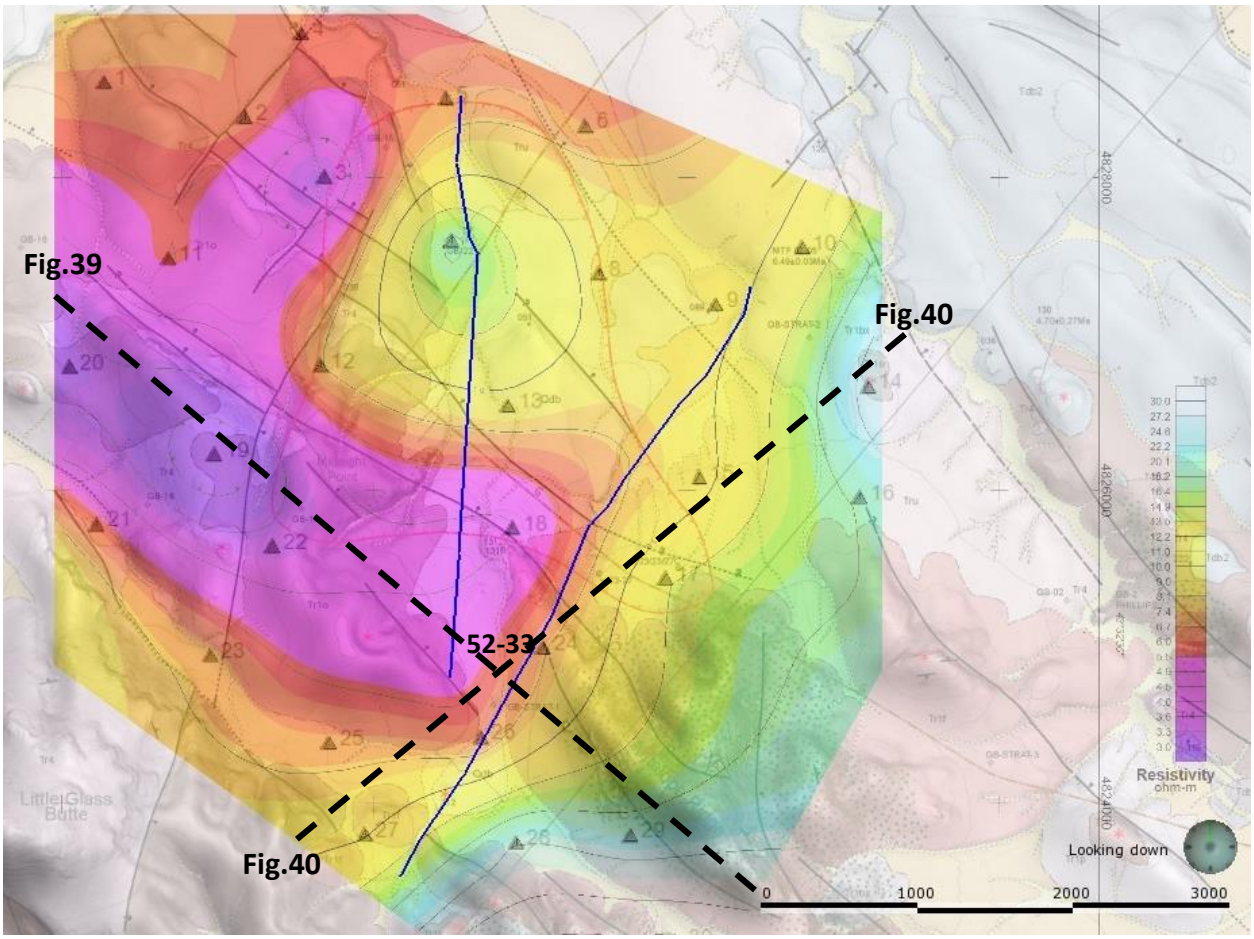

Figure 38: 1D inversion results of static-corrected determinant resistivity for an elevation of 1000m with mapped structures and MT stations in the Midnight Point area. Location of cross-sections for Figure 39 and Figure 40 are shown as dashed line focusing

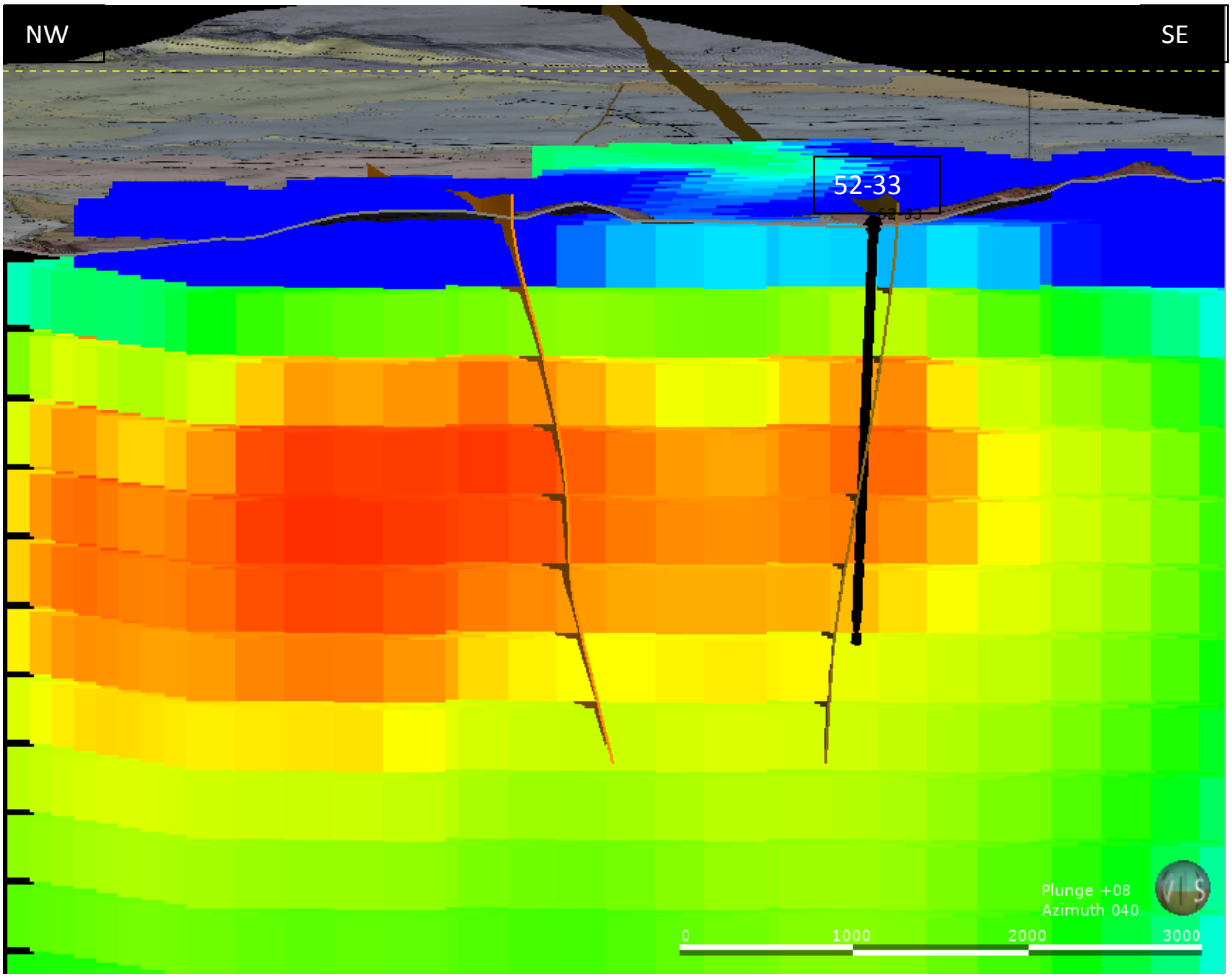

Figure 39: Resistivity voxel of the one dimensional MT inversion showing interpreted fault planes and drill hole 52-33 looking NE

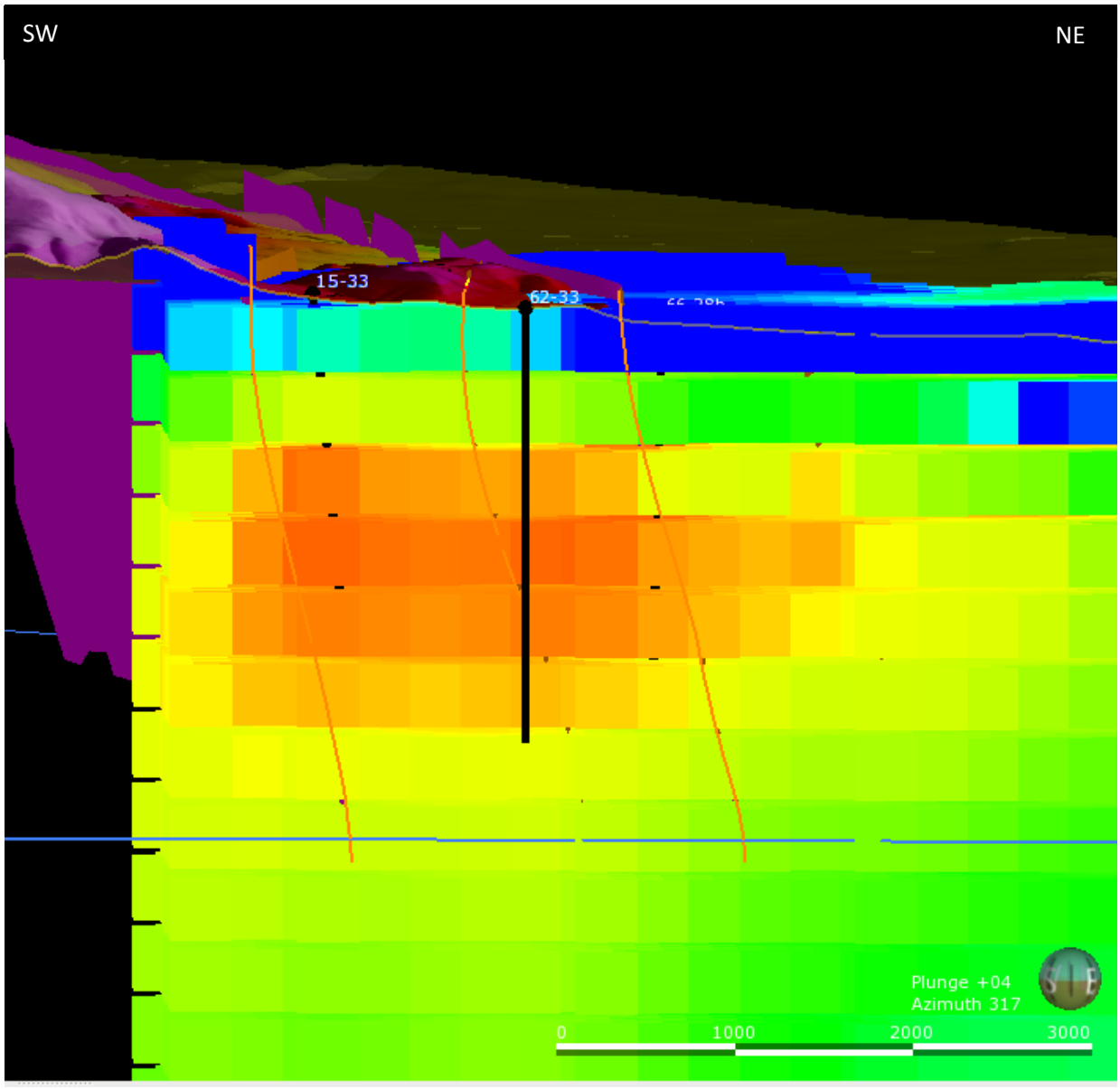

Figure 40 Resistivity voxel of the one dimensional MT inversion showing interpreted fault planes and drill hole 52-33 looking NNW

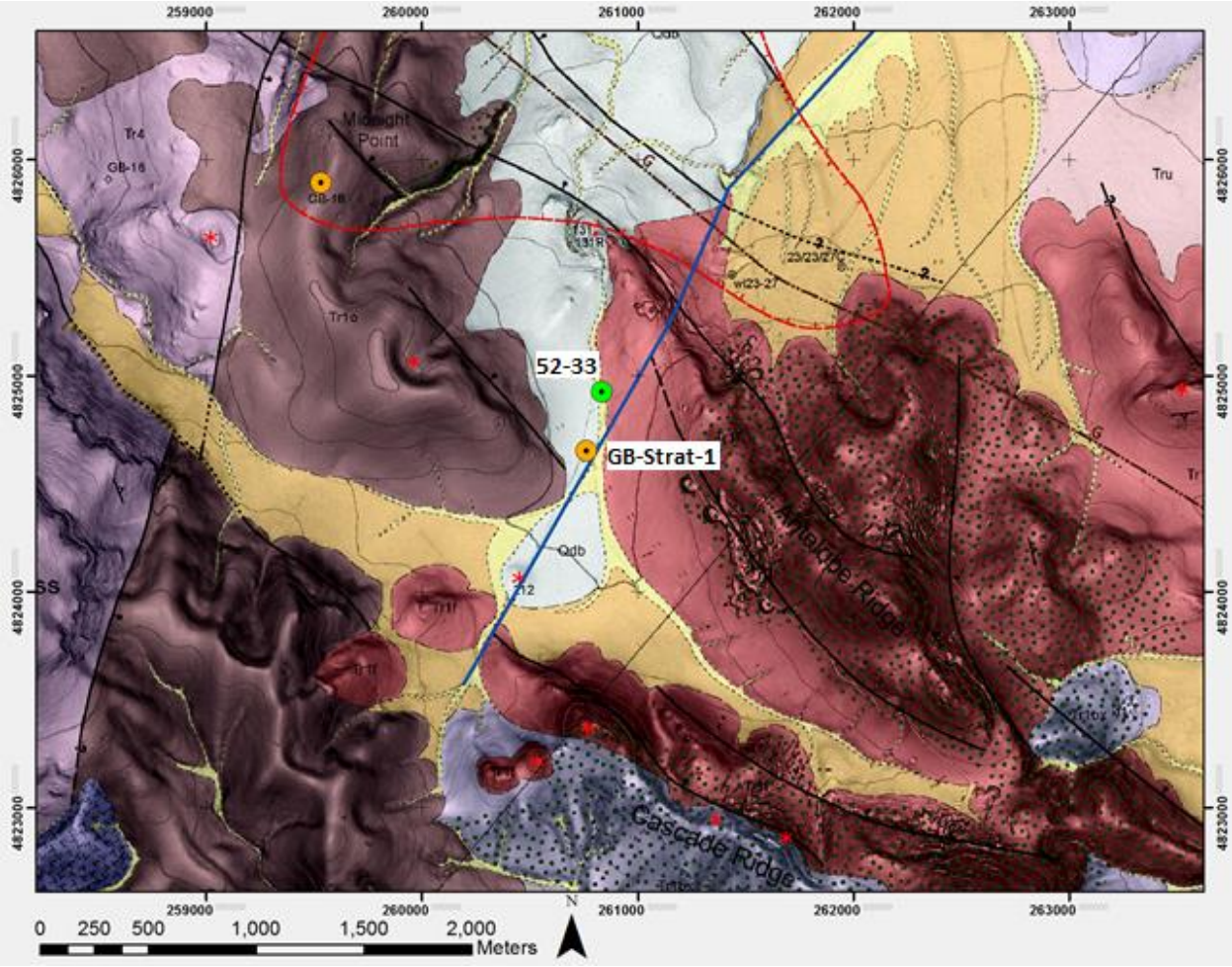

Figure 41: Geological map showing the location of drill hole 52-33, STRAT-1 and GB-18 well

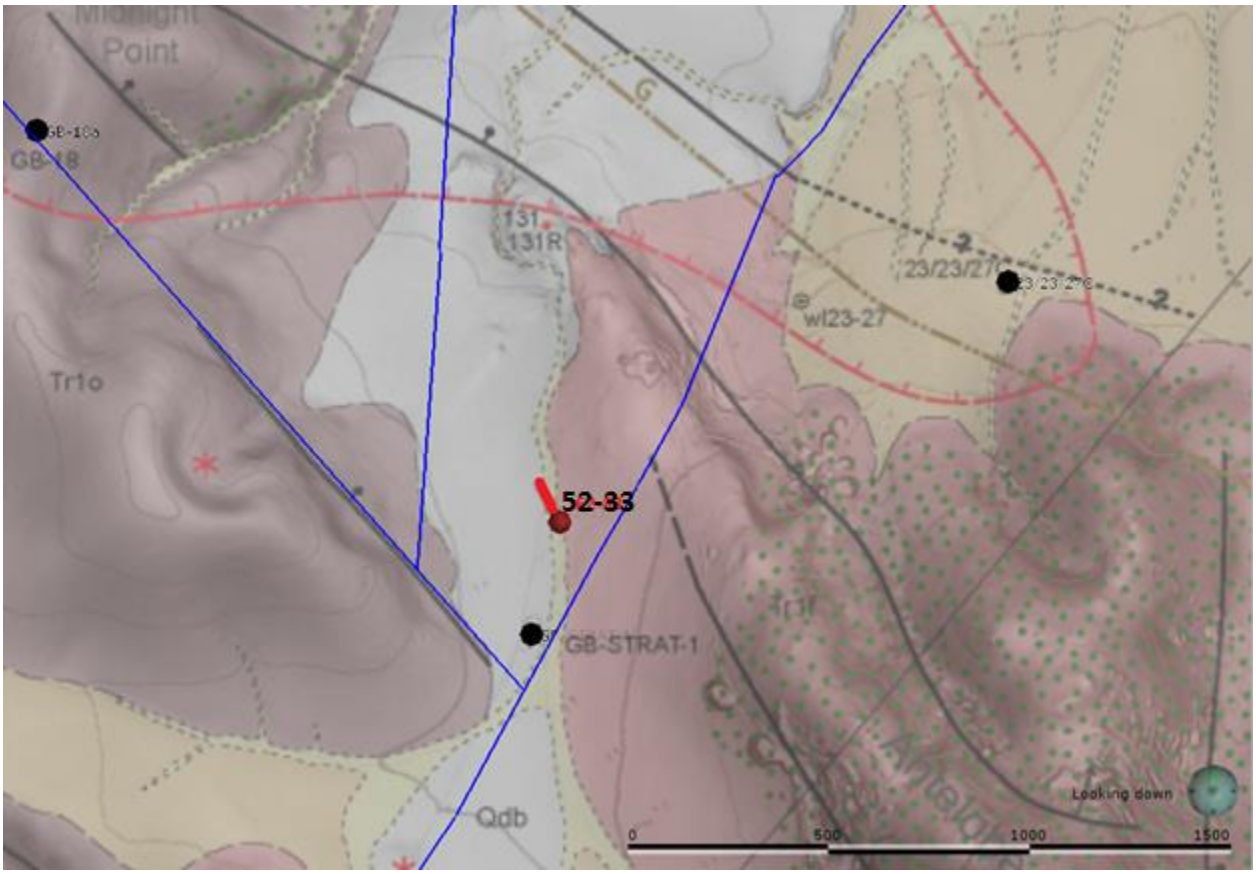

Figure 42: Plan view map showing the path of 52-33, existing drill holes, and the geological map.

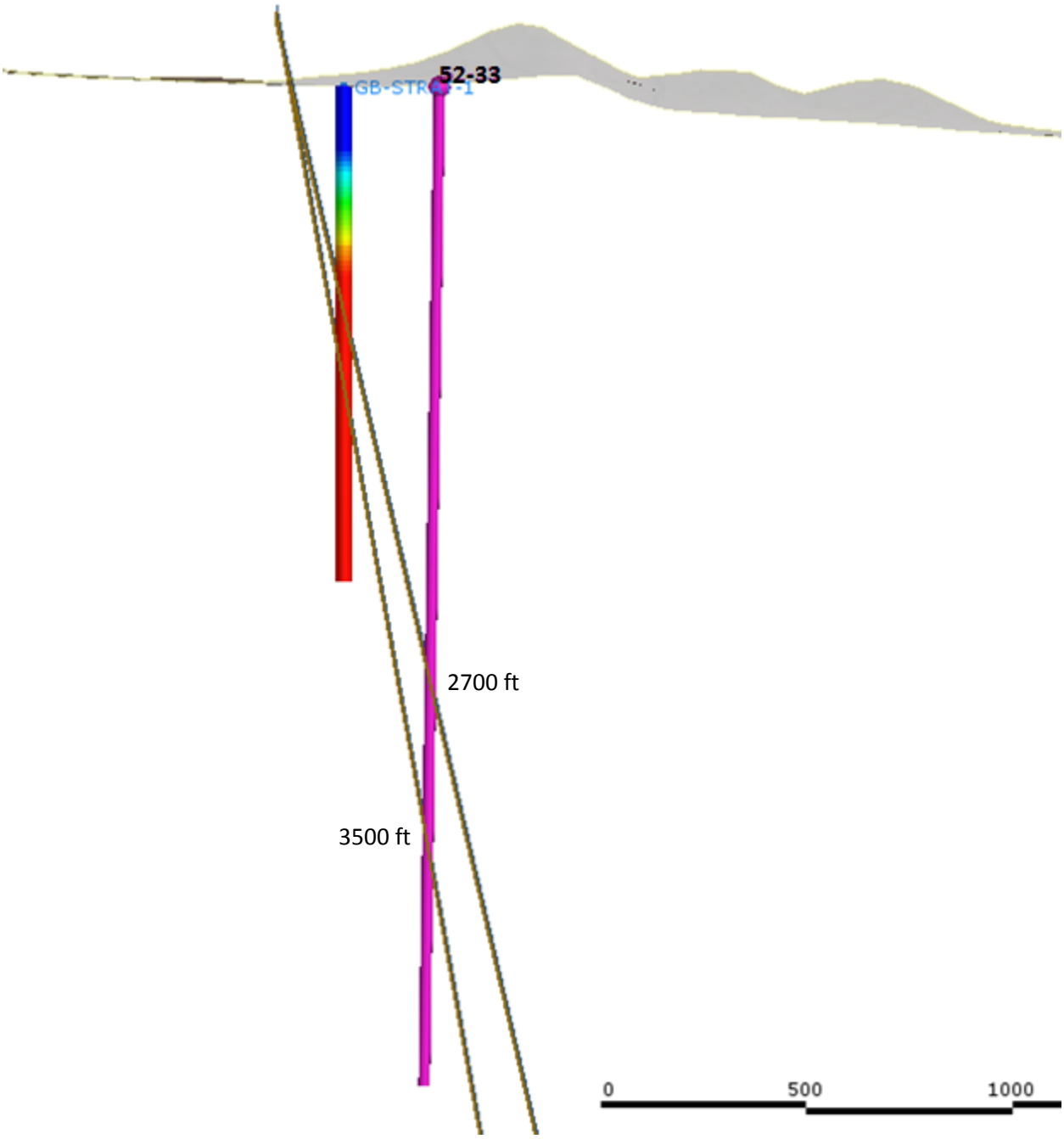

Figure 43: Cross-section, looking towards the NW, oriented parallel to the geophysically-defined structure and perpendicular to the targeted NW trending structure, showing modeled drill hole 52-33 and STRAT-1 well intersecting the NW trending structure with a dip of 65 degrees and 70 degrees.

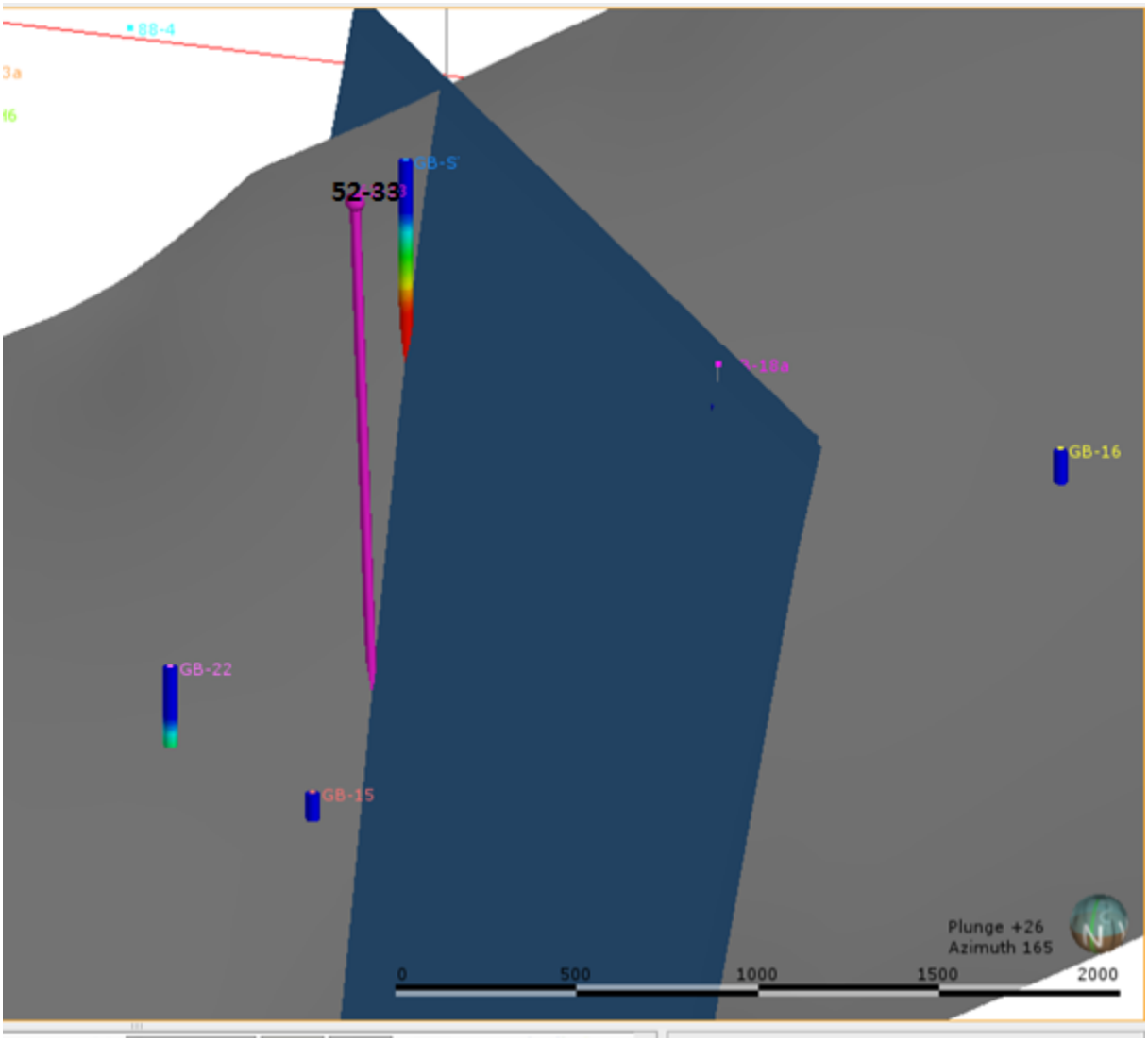

6.0 Figure 44: Perspective view looking down and towards the SE at modeled drill hole 52-33, STRAT-1 well, and the fault intersection of the targeted NW trending structure and the geophysically defined NE trending structure.How innovative technologies were used to target well sites

The primary objective of this project was to combine a suite of high resolution geophysical and geochemical techniques to reduce exploration risk by characterizing fault geometries and relationships. Surveys including LiDAR, Hyperspectral, gravity, aeromagnetics, and magnetotellurics were conducted, interpreted, and combined into a single model along with historic down-hole lithology and temperature data to achieve this goal. The most useful surveys for advancing our knowledge of the structural relationships were the LiDAR, gravity, and magnetics surveys. The LiDAR improved the geologic and structural mapping because features

such as minor breaks in slope could be used to better constrain lithologic contacts or subtle faults that were not clearly identified using traditional methods. The LiDAR data were also very valuable in defining cross-cutting relationships and therefore relative ages of geologic features.

The gravity and magnetic surveys were useful in confirming the location and orientation of faults identified by geological mapping and LiDAR data, as well as identifying additional structures that cannot be observed at the surface. These two geophysical methods are complimentary since magnetic surveys map variations in magnetic susceptibility, which can image structures within volcanic lithologies; whereas gravity surveys map changes in density related to rock type at depth. Strong gradients in the gravity and magnetic data confirm that structures identified by geological mapping and LiDAR continue at greater depth, which is very important information when selecting drill targets.

Calculated geophysical maps were compiled using the latest version of Oasis Montaj from Geosoft Inc. Oasis Montaj is considered the leading exploration software technology for processing, mapping and analyzing large volumes of geophysical data in one integrated environment. With the recent addition of the VOXI Earth Modeling inversion extension it is possible to perform 3D inversions of magnetic and gravity data seamlessly within the software platform. 3D models of physical properties that used to take several hours of computing using separate software packages can be generated within the Oasis Montaj platform in minutes by utilizing cloud computing technology.

After processing, all geophysical and geological data sets were integrated to a comprehensive 3D model using Leapfrog Geothermal software. Leapfrog Geothermal was specifically developed for geological modeling and exploration of geothermal resources. Using this software, three dimensional curvilinear fault planes were created to honor an integrated interpretation of all available data sets. These fault planes provide drilling targets that are anticipated to provide enhanced permeability for high temperature fluid flow. As drill holes are completed and other new data sets become available the geological model will be continuously updated within this software platform. In addition, the geologic model can be exported to the industry-standard Tough2 reservoir modeling software following successful drilling.

7.0 Drilling

7.1 Well Location

The existing Strat-1 and the shallower GB-18 displayed both displayed high temperature gradients to depth – if they were to maintain this gradient both wells would reach a temperature of 150°C at a depth of only 3000 ft. (map figure 45, temperature profiles figure 46).

Ormat's conceptual model was that fluids flow up along a NW-striking fault that connects GB-18 and Strat 1 and this fault's intersection with NNE-striking faults. The high shallow gradients to the north are a result of outflow along faults with both orientations. This hypothesis was supported by 1) the magnetic low along the north-trending graben 2) the low resistivity along these structures at depth, and 3) the rapid decline in temperature gradient to the south. 52-33 was targeted to intersect these structures. This well was originally called 62-33 but was moved slightly and renamed to avoid being located on seasonal drainage, with a surface location of 260781mE 4824999mN (UTM NAD83 Zone 11), NW ¼ NE ¼ Section 33, T23N, R23E.

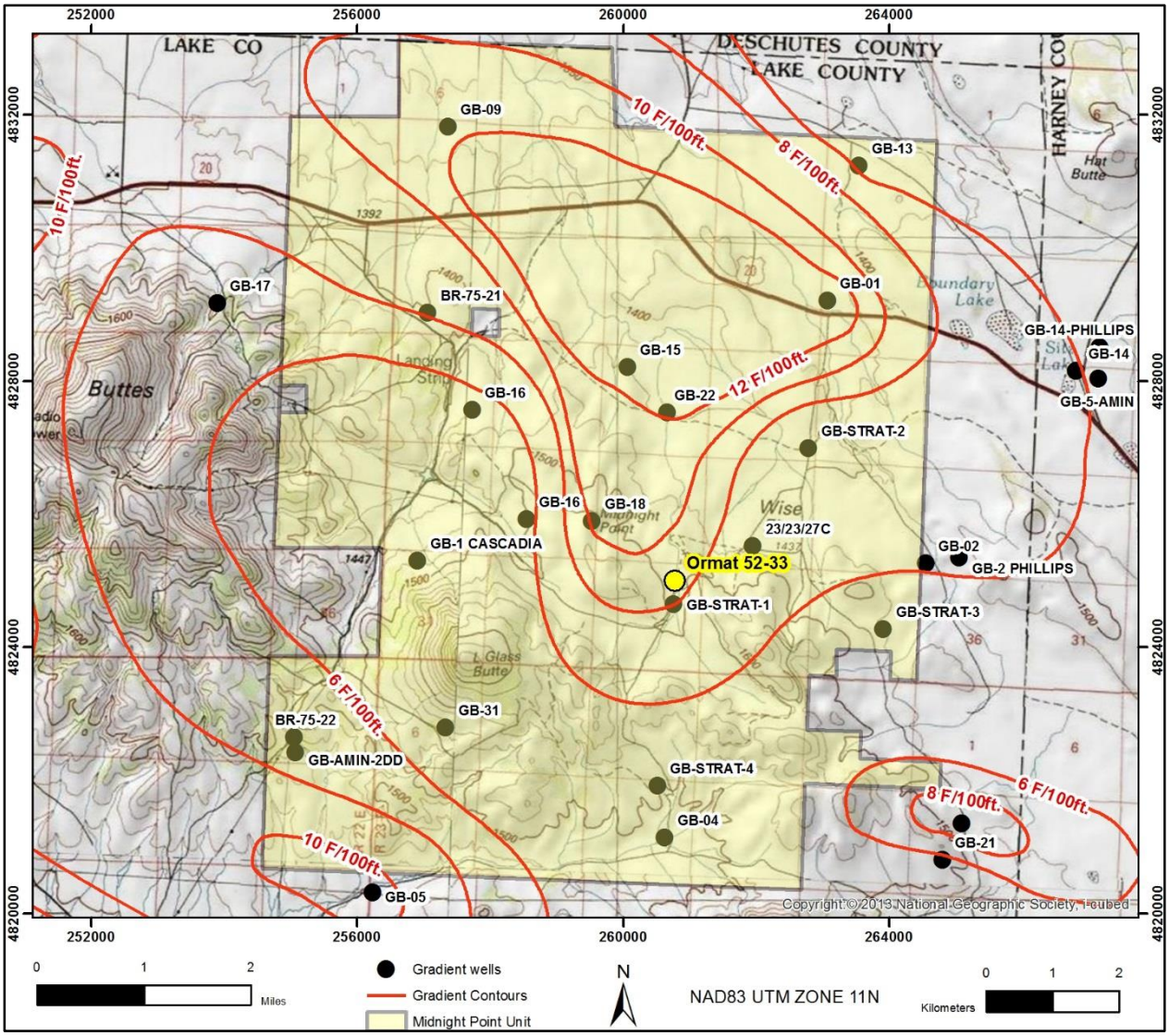

Figure 45: Map of the Midnight Point prospect showing Phillips wells, temperature gradients, and 52-33

7.2 Well Results

52-33 encountered basalt for the first 110 ft. before moving into a sedimentary package of clays, sands, and gravel to 270'. From 270-500 ft. there were no returns, and then the well encountered alternating packages of volcanics including obsidians, rhyolites, tuffs, and basalts to 3000 ft. TD (see core log at end of this report). There were losses in the shallow portion of the well below 1000 ft., likely associated with volcanics and their contacts, however the target zone from 2000-3000 ft. did not experience significant losses, suggesting a lack of permeability. Abundant fracturing was found from 2525-2640 ft., and 2770-2855, but the majority were chlorite or calcite filled (Figure 47), or unaltered and closed. This fracturing was at the depth predicted by our

modeling and may be associated with the target structures. Chlorite, hematite, and calcite alteration were found filling vugs and fractures; however the abundant silica alteration often associated with deposition by active geothermal fluids was not seen.

Temperature gradient in 52-33 was roughly 10° F/100ft to ~1500 ft, mirroring the Phillips GB-18 and Strat-1 wells. After that point, the gradient decreased to near isothermal conditions below 2000 ft, with a final bottom hole temperature of only 203°F. Based on these results, it is possible that if either of the Phillips wells had been as deep they also would have gone isothermal.

Due to a lack of deeper fault targets, closed and filled fractures through the target zone, and low temperature, the decision was made to TD the well at 3000 ft. 52-33 was completed with 7 inch K-55 BTC casing to 39 ft., followed by 4.5 inch K-55 VJF casing to 495 ft. From 495 ft. to 3000 ft. TD, the well was left open-hole with HQ 3.895 inch diameter (Figure 48).

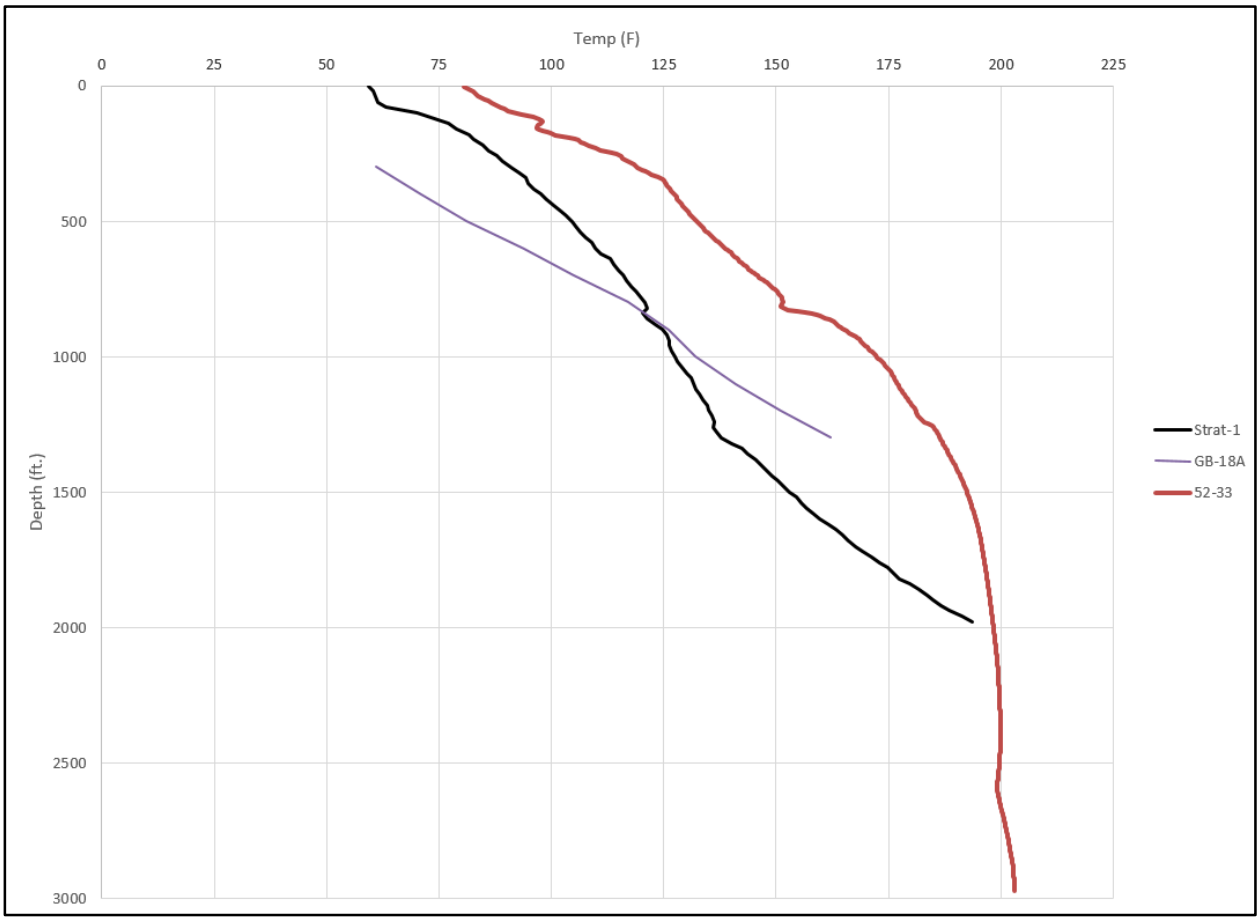

Figure 46: Temperature profiles of Phillips Strat-1 and GB-18, alongside Ormat 52-33

A.)

B.)

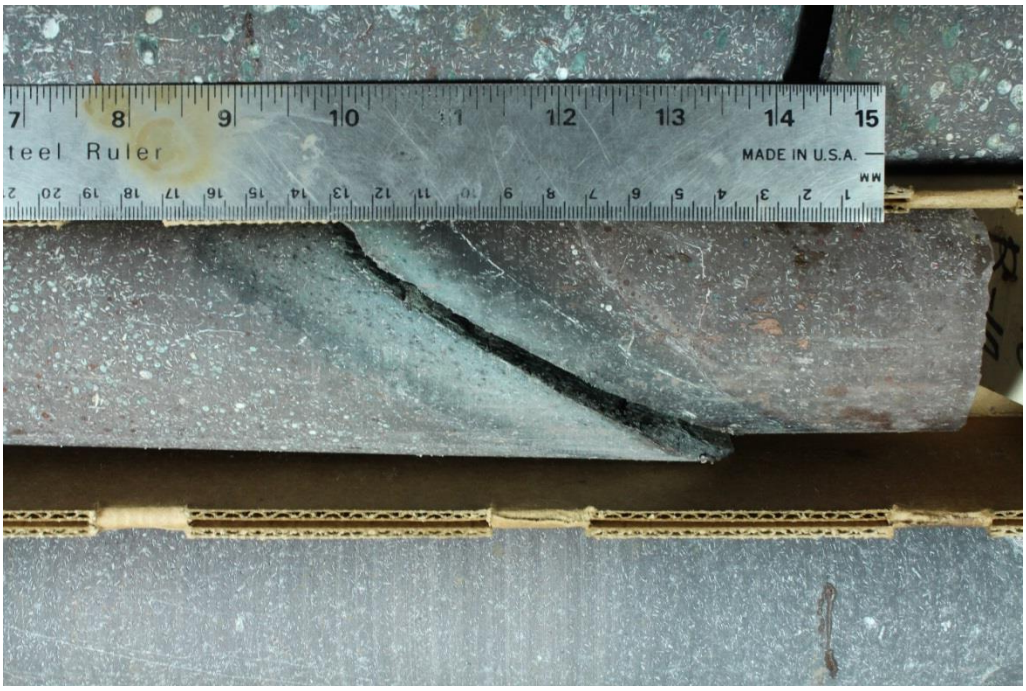

Figure 47: Examples of calcite and chlorite filled fractures in the core at A.) 2533 ft. and B.) 2779 ft.

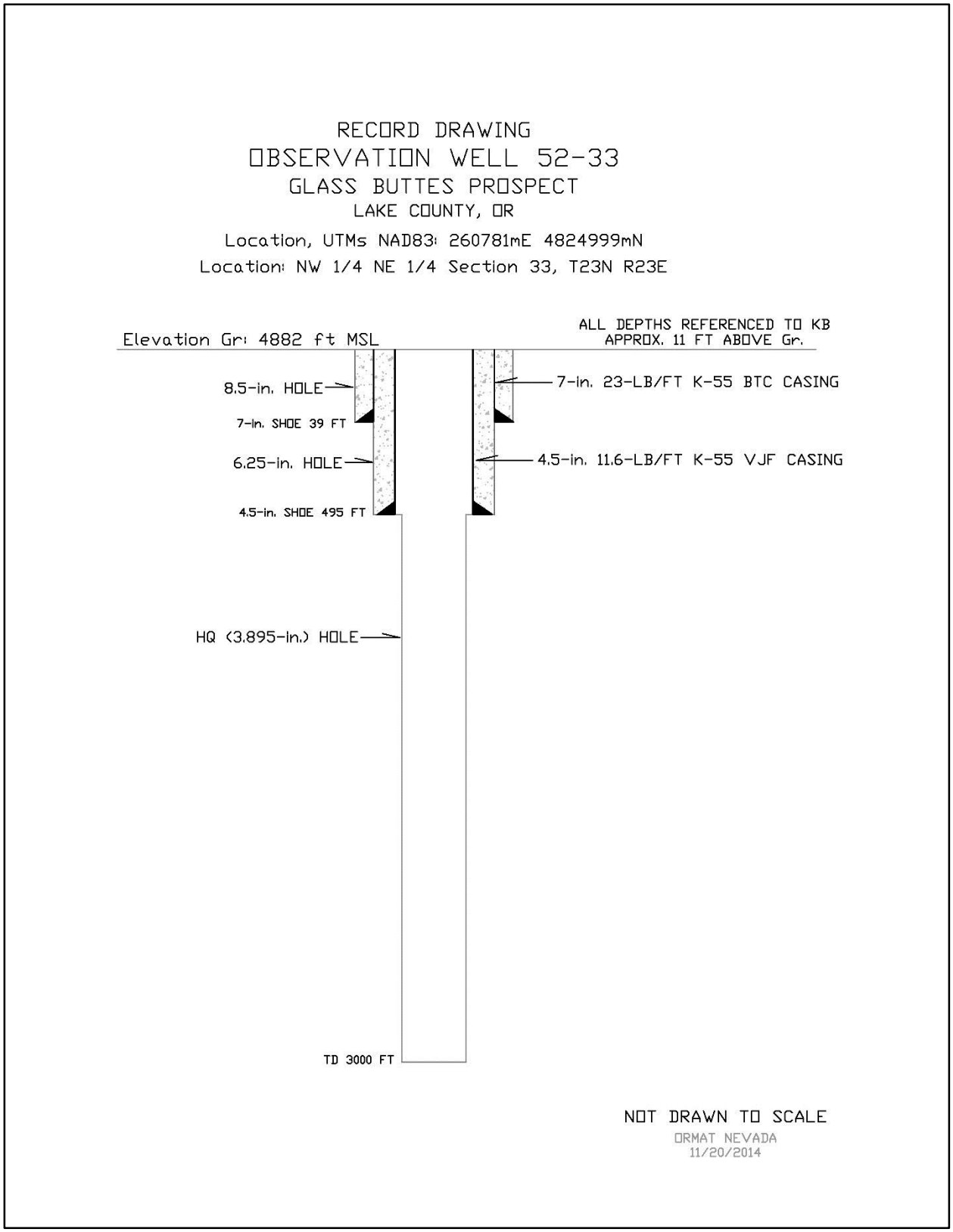

Figure 48: Well diagram of Ormat 52-33

8.0 Lessons learned

The exploration program for Midnight Point improved our understanding of the prospect and therefore reducing the risk of further exploration drilling. The most innovative technologies, LiDAR, 3D geologic modeling, and hyperspectral are combined with more traditional methods of gravity, magnetics, geologic mapping and MT. The LiDAR-based, highly detailed geologic mapping and the collection of closely-spaced gravity early in the project should also be considered innovative as these are historically rare in geothermal developments.

Interpretation of the LiDAR identified many geologic features not previously identified, and more importantly improved our ability to quantify fault interactions. Ormat has already significantly increased our use of LiDAR around the world based on the perceived value of these results. Similarly, when we wrote the original Glass Buttes proposal, 3D geologic modeling was at an early stage at Ormat. Since that time and partly driven by the value demonstrated at Glass Buttes, especially in conveying results to management, we have created 3D models of most of our exploration and development fields using Leapfrog software. The correlation between features observed on the surface with those identified by geophysics and previous temperature gradient drilling have driven our recommendation for first drilling targets.

While the magnetotelluric method provided some useful information in confirming the general location of structures in the Midnight Point area, the survey design and inherent limitations on the inversion method based on the station spacing made it difficult to improve interpretations concerning structural dip at depth. Since resistivity contrasts were observed near mapped structures additional MT lines designed with 100m station spacing could provide sufficient resolution for a more detailed analysis of structures at depth. If a project at Glass Buttes were to move forward, detailed MT lines should be completed over the most important structures with two dimensional inversions to gain a better understanding of the fault geometry at depth.

Hyperspectral data improved our understanding of minerals present, but was not a significant factor in siting wells, especially following the interpretation that alteration predates the most recent volcanic flows (Boschman, 2012). If we were restarting the exploration program and considering the hyperspectral survey cost, we would most likely hold off until the rest of the program was completed.

The drilling results of exploration well 52-33 improved our geologic understanding of the prospect. Fractures were encountered in the expected target interval however chlorite, hematite, and calcite alteration were found filling vugs and fractures, reducing permeability. The abundant silica alteration often associated with deposition by active geothermal fluids was not

seen. The shallow (<2000 ft.) high temperature gradient recorded in the nearby Strat-1 and GB-18A wells was encountered in 52-33, however temperatures quickly went isothermal as the well approached greater depths. These results may indicate that the target area is near the edge of the geothermal system. Future wells may target higher temperature gradients to the north to explore for upflow and higher temperatures, such as the northern temperature gradient anomaly in shown **Figure 3**. This study was successful in increasing our understanding of the prospect, nonetheless unknown deep thermal conditions make exploring for blind geothermal systems a risky endeavor.

Resulting Publications

Boschmann, Darrick E. Structural and volcanic evolution of the Glass Buttes area, High Lava Plains, Oregon, Oregon State University Collections: http://hdl.handle.net/1957/36266

Boschmann, D.E., J. Dilles, A. Meigs and P. Walsh (2011). Structural and volcanic evolution of the Glass Buttes area, Oregon. Transactions – Geothermal Resources Council 35-1: 727-729

Walsh, P.; Martini, B.; Lide, C.; Boschmann, D.; Dilles, J. H.; Meigs, A. Multiple data sets converge on a geologic structural model for Glass Buttes, Oregon geothermal prospect. American Geophysical Union, Fall Meeting 2010, abstract #V13B-2360

Walsh, Patrick, Martini, Brigette, Lane, Richard, and Spragg, Kirk. 3D geologic modeling improves well targeting in Glass Buttes, Oregon. GSA annual Meeting, Fall 2011.

Bibliography

Benoit, W. R. (1981). *The results of intermediate depth drilling at the Glass Buttes Prospect, Lake County, Oregon.* Phillips Petroleum internal report.

Berri, D. A. (1982). *Geology and hydrothermal alteration, Glass Buttes, Southeast Oregon.* M.S. Thesis, Portland State University.

Boschman. (2012). *Structural and Volcanic Evolution of the Glass Buttes Area, High Lava Plains, Oregon.* M.S. Thesis, Oregon State University.

Crider, J. G., & Pollard, D. D. (1998). Fault linkage: three-dimensional mechanical interaction between echelon normal faults. *J. Geophy. Res., 103*(24), 373–24,391.

Ford, M. (n.d.). *Unpubished data.* Department of Geosciences, Oregon State University.

Glassley, W. E. (2010). *Geothermal energy.* Boca Raton: CRC Press.

Haugerud, R., Harding, D. J., Johnson, S. Y., Harless, J. L., Weaver, C. S., & Sherrod, B. L. (2003). High-resolution topography of the Puget Lowland, Washington—A bonanza for earth science. *GSA Today, 13*, 4–10.

Johnson, K. W., & Ciancanelli, E. V. (1989). Geothermal exploration at Glass Buttes, Oregon. *GRC Transactions, 7*, 169-174.

Johnson, M. J. (1984). *Geology, alteration and mineralization of a silicid volcanic center, Glass Buttes, Oregon.* M. S. Thesis, Portland State University.

Jordan, B. T., Grunder, A. L., Duncan, R. A., & Deino, A. L. (2004). Geochronology of age-progressive volcanism of the Oregon High Lava Plains: Implications for the plume interpretation of Yellowstone, 109. *J. Geophys. Res.*, 109.

Lawrence, R. (1976). Strike-slip faulting terminates the Basin and Range Province in Oregon. *Geological Society of America Bulletin, 87*, 846-850.

McKee, E. H., & Walker, G. W. (1976). Potassium-argon ages of late Cenozoic silicic volcanic rocks, southeastern Oregon. *Isochron West, 15*, v.15, p. 37–41.

Peacock, D., & Sanderson, D. (1994). Geometry and development of relay ramps in normal fault systems. *American Association of Petroleum Geologists Bulletin, 78*, 147-165.

Roche, L. R. (1987). *Stratigraphic and geochemical evolution of the Glass Buttes complex, Oregon.* unpub. Masters Thesis, Portland State Univ.